8-2011

Echogenic Liposomes For Nitric Oxide Delivery And Breast Cancer Treatment

Soo Yeon LEE Female

ECHOGENIC LIPOSOMES FOR NITRIC OXIDE DELIVERY

AND BREAST CANCER TREATMENT

by

Soo Yeon Lee, B.S.

APPROVED:

_____
[Hyunggun Kim, PhD]

_____
[Shao-Ling Huang, MD, PhD]

_____
[Emil Martin, PhD]

_____
[Iraida G Sharina, PhD]

_____
[Gary E. Gallick, PhD]

_____
[Heinrich Taegtmeyer, MD, DPhil]

APPROVED:

_____
Dean, The University of Texas

Graduate School of Biomedical Sciences at Houston

ECHOGENIC LIPOSOMES FOR NITRIC OXIDE DELIVERY AND BREAST CANCER TREATMENT

A

THESIS

Presented to the Faculty of
The University of Texas
Health Science Center at Houston
and
The University of Texas
M. D. Anderson Cancer Center
Graduate School of Biomedical Sciences
in Partial Fulfillment

of the Requirements

for the Degree of

MASTER OF SCIENCE

by

Soo Yeon Lee, B.S.
Houston, Texas

August, 2011

ACKNOWELDGEMENT

I would like to express my great appreciation to Dr. Kim for giving me an opportunity to pursue my master's degree and for allowing me to step into the world of science. I appreciate all his efforts and concerns in giving me as a student researcher as well as continuous encouragement.

I am truly thankful for my excellent committee members for their generous support by providing valuable suggestions on my research. I would like to express my appreciation to Dr. Huang whose constant help and dedication has been crucial from the initial to the final study of my research. I truly appreciate to Dr. Emil's constant suggestions and supports on my research and his motivating me to be a true scientist. I would like to express my great appreciation to Dr. Sharina who has provided me valuable insights on my professional and personal life. My appreciation goes to Dr. Taegtmeyer whose support always encourages me to pursue my professional life. I truly appreciate Dr. Gallick's supports and comments on my research as well as for providing me a motivation to study on cancer metastasis.

I would like to truly thank Dr. McPherson and all members of his laboratory. His concern and guidance has encouraged me to develop my research and to become an excellent leader like him. I would like to thank you; Dr. Klegerman, Joy, Melanie, Beverly, George and Dr. Tao, Dr. Laing, Dr. Kee, and Dr. Rim for their great friendship and advice. It has been my great pleasure to get to know all of you.

Lastly, a special thanks goes to my valuable family and friends for their love and assistance. I would like to thank my parents and sister for believing in my potential. My special thanks goes to my close friends Amy Han and Hyojin Cho for always being there for me and their constant support. I would not have been able to finish this without their encouragement.

ECHOGENIC LIPOSOMES FOR NITRIC OXIDE DELIVERY

AND BREAST CANCER TREATMENT

Publication No._____

Soo Yeon Lee, B.S.

Supervisory Advisor: Hyunggun Kim, Ph.D.

Liposomes, also known as nontoxic, biodegradable, and non-immunogenic therapeutic delivery vehicles, have been proposed as a carrier for drugs and antitumor agents in cancer chemotherapy. Echogenic liposomes (ELIP) have the potential to entrap air or bioactive gas to enhance acoustic reflectivity in ultrasound and are used as a contrast agent. The innovative part of this study is based on a novel concept to encapsulate nitric oxide (NO) gas into ELIP, deliver it to breast cancer cells, and control its release via direct ultrasound exposure. Studies on the effect of NO in tumor biology have shown that a high levels of NO (> 300 nM) leads to cytostasis or apoptosis by decreasing the translation of several cell cycle proteins and stimulating cancer cell death by activating the p53 pathway. The *central hypothesis* is that NO gas can be packaged and delivered through a delivery methodology to breast cancer cells to facilitate tumor regression with minimal systemic toxicity. The *primary goal* of this thesis is to develop an echogenic liposomal solution that has the ability to encapsulate NO, to release NO locally upon ultrasound exposure, and to induce breast cancer cell death. NO-containing echogenic liposomes (NO-ELIP) were prepared by the freezing-under-pressure method previously developed in our laboratory. It was necessary to evaluate stability of NO-ELIP and release of NO from NO-ELIP by measuring echogenicity using intravascular ultrasound images. Breast cancer cell lines, MDA-MB-231 and MDA-MB-468, were selected to investigate the cytotoxic effects of NO

liberated from NO-ELIP and their response to NO concentration. Ultrasound-triggered NO release from NO-ELIP using ultrasound activation was studied. It was demonstrated that NO-ELIP remained stable for 5 hours in bovine serum albumin. Delivery of NO using NO-ELIP induced cytotoxicity and programmed cell death of MDA-MB-231 and MDA-MB-468 after 5 hours of incubation. Enhancement of the NO-ELIP effect for therapeutic application was observed with ultrasound activation. This work demonstrates that NO-ELIP can incorporate and deliver NO to breast cancer cells providing increased NO stability and ultrasound-controlled NO release. Improved therapeutic effect with the use of NO-ELIP is expected to be found for breast cancer treatment.

TABLE OF CONTENTS

LIST OF FIGURES

LIST OF ABBREVIATIONS

ATP	Adenosine triphosphate
Bak	BCL2-antagonist/killer
Bax	BCL-2 associated X protein
BCC	Breast cancer cell
BCL-2	B-cell lymphoma 2
BID	BH3 interacting domain death agonist
BIM	BCL-2 interacting mediator of cell death
BSA	Bovine Serum Albumin
CDK	Cyclin-dependent kinase
DC-Cholesterol·HCl	3β-[N-(N',N'-dimethylaminoehane)-carbamoyl] cholesterol hydrochloride
DMEM	Dulbecco's modified eagle medium
DMSO	Dimethylsulfoxide
DPPC	1,2-Dipalmitoyl-sn-glycero-3-PhosPhoCholine
DPPE	L-α-DipalmitoyPhosPhati-dylEthanolamine
DPPG	1,2-Dipalmitoyl-sn-glycero-3-[PhosPhor-rac-l-Glycerol]
Egg PC	Egg L-α-Phosphatidylcholine
EGFR	Epidermal growth factor receptor
ELIP	Echogenic liposome
ER	Estrogen receptor
FGF	Fibroblast growth factor
Her-2	Human epidermal growth factor receptor 2
IC_{50}	Half-maximal inhibition concentration
IVUS	Intravascular ultrasound

MGSV	Mean gray scale value
MTT	3-(4,5-Dimethylthiazol-2-yl)-2,5-diphenyltetrazolium bromide
NO-ELIP	NO-containing echogenic liposome
MOMP	Mitochondria outer membrane permeabilization
PBS	Phosphate buffer saline
PDGF	Plate-derived growth factor
PLD	Pegylated liposomal doxorubicin
PR	Progesterone receptor
pRb	Retinoblastoma protein
PUMA	The p53 upregulated modulator of apoptosis
tPA	Tissue plasminogen activator
UCA	Ultrasound contrast agent
UV	Ultraviolet
VEGF	Vascular endothelial growth factor

CHAPTER I

General Introduction

1.1. Epidemiology of breast cancer

Breast cancer is the most common type of cancer occurring among women in the United States (1). Breast cancer also remains principal cause of death among women aged 30-55 years (2). According to survey from the American Cancer Society, there were an estimated 207,090 of new breast cancer cases in 2010. About 28% of women are expected to be diagnosed with breast cancer in their life time in the United States (1).

In 2002, Baum and Schipper reported that the increase incidence of breast cancer is mainly related to ages, environmental risk factors, and genetic factors (2). Approximately 50 % of breast cancers occur in women aged 50-64 years and 30 % occur in women over the age of 70 (2). In terms of environmental factors, there is a higher incidence in women from developed countries (2, 3). However, the incidence rates are rapidly increasing in developing countries. A family history of breast cancer, as a genetic factor, is also accepted as a risk factor for breast cancer (2). Women with a first-degree relative with breast cancer have 2-3 fold increase in the risk of breast cancer (2, 3).

Breast cancer is a heterogeneous disease since there are several prognostic factors and clinical forms (4). There are numerous factors to influence the incidence of breast cancer and its origin (5,6). It is important to understand breast microenvironment in order to elucidate the physiological features and development of breast cancer (6).

1.2. Anatomy of breast

The breast consists of glandular, fatty and fibrous tissue positioned over the pectoral muscles of the chest wall (7). As shown in Fig 1.1, the glandular tissues are composed of 15-20 lobes containing numerous lobules known as milk glands (4). Lobules are linked by ductules that transport milk from lobules to the nipple (7). Lobules and ducts are surrounded by two layers of fibrous tissue; a superficial layer and thicker deep layer connected by Cooper's ligaments (2). It is essential to understand the surrounding tissue of breast because breast cancer is associated with tissue sites of adenocarcinoma (8). Additionally, tissue microenvironment can profoundly affect on the incidence of invasive breast cancer (8).

Most malignant breast cancers arise from a group of abnormal cells in ducts and lobules shown in Fig 1.2 (2). The origins of breast have invaded to surrounding tissues which support the lobules and ducts of the breast (5). About 90 % of breast cancer consist of invasive ductal cancer (5). Invasive lobular carcinoma is the second most common type of breast cancer (2). Lobular carcinoma in situ is not invasive, however, there is rapid increase of abnormal cell proliferation in the breast lobule (2). When the origin of breast cancer is well understood, breast cancer treatment would be more effective (2).

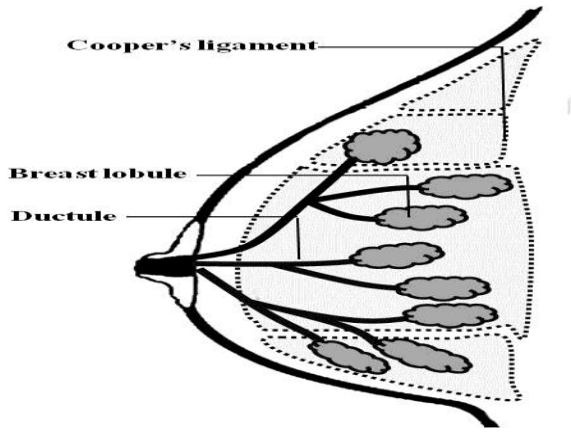

Figure 1.1 Structure of normal breast (2)

Adapted from Baum, M.

The diagram depicts the anatomy of breast. Breast lobules are linked to ductules to transport milk to the nipple. Lobules and ducts are surrounded by Cooper's ligaments which are connected to fibrous tissue. The intraductal system is erratic and strongly correlated with the incidence of breast cancer.

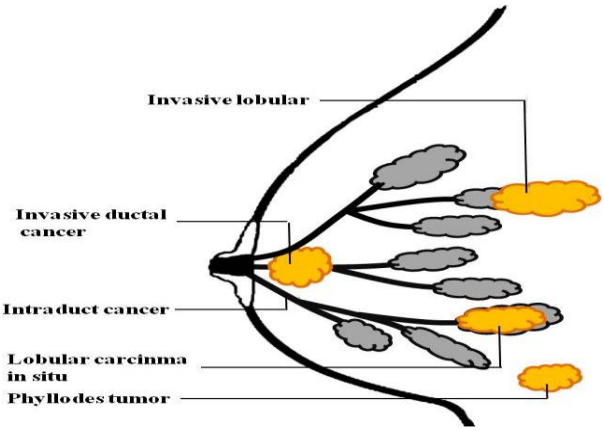

Figure 1.2 Types of breast cancer (2)

Adapted from Baum, M.

Invasive breast cancer are generated from lobules and ductules, which invade the surrounding tissue. Lobular carcinoma in situ stimulates abnormal cell proliferation, yet does not metastasize to breast tissues around the ducts and lobules.

1.3. Conventional breast cancer therapy

1.3.1. Hormone therapy

Breast cancer cells express proteins called estrogen receptor (ER) and progesterone receptor (PR) (9). ER can modulate breast cancer cell growth in response to one of the sex hormone, estrogen, and its overexpression leads to faster breast tumor growth (9). Hormone therapy, known as adjuvant endocrine therapy, is used to treat pre-menopausal women with hormone receptor (HR)-positive breast cancer and post-menopausal women who have aromatase inhibitor (10). ER, a transcription factor, is one of the nuclear hormone receptors superfamily that regulates transcription of target genes (11). When ER binds to estrogen, ER undergoes receptor dimerization and activation. Ligand-bound ER translocates to the nucleus followed by full activation of transcription of genes, which can stimulate cancer growth.

Tamoxifen has been commonly used as an anti-estrogen drug for invasive breast cancer treatment (11, 12). Tamoxifen binds to ER, prevents ER from interacting with estrogen, and reduces breast cancer cell proliferation (11). Hormone therapy with tamoxifen in patients who suffer from ductal carcinoma in situ (DCIS) decreases the risk of developing invasive cancer (10).

Hormonal therapy reduces relapse of breast cancer and extends patient survival by 10 years (9, 13). However, it has been reported that the clinical effect of tamoxifen relies on ER/PR status (9). ER/PR-positive breast tumor has about 80 % chance to respond to tamoxifen, while there is 40 % chance in response to tamoxifen with the expression of ER (10). The combination of hormone therapy such as tamoxifen and goserelin is needed to overcome the limitation of a single hormone therapy (14).

1.3.2. Immunotherapy

The prevalence of human epidermal growth factor receptor 2 (Her-2) is expressed in approximately 25 % of breast tumors (9). Her-2 has potential to be used as a prognostic marker for the detection of early invasive breast cancer (15). The overexpression of Her-2, a receptor tyrosine kinase, on the surface of a breast cancer cell membrane induces cell proliferation through the Ras-Raf-mitogen-activated protein kinase (MEK)/ERK pathway as well as survival signaling through phosphorylation of Akt followed by the onset of transcription of growth-associated gene (9).

Trastuzumab, anti-Her-2 Mab; Herceptin, is a monoclonal antibody and targeted anti-Her-2 oncoprotein and is commonly used to treat patients with invasive breast cancer (16). Trastuzumab inhibits Her-2 dimerization by binding the extracellular domain of Her-2 and reducing high proliferation rate (9). In a phase comparison trial, trastuzumab in combination with chemotherapy has improved overall survival for patients who have Her-2-positive metastatic breast cancer (17). The addition of trastuzumab to chemotherapy leads to better results such as a 25.1 more months median survival than standard chemotherapy alone (9, 17). Adjuvant chemotherapy with trastuzumab has become standard in patients with Her-2-positive early-staged breast cancer and shown the improvement of response rate and overall survival (15).

1.3.3. Anti-cancer therapy

Cytotoxic drugs affect the inhibition of malignant cell proliferation and growth (18). Anthracyclins, one of cytotoxic drugs, is widely used in chemotherapy for early-staged and advanced breast cancer (19) . However, the cumulative anthracyclines dose induces cardiac toxicity and myelosuppession that in turn limits medical use (18, 20). Therefore, many studies

have focused on preserving cytotoxic drug delivery systems for better drug safety profiles and therapeutic efficacy (20).

Liposomal doxorubicin has been approved to prolong circulation of drugs and utilized for the treatment of breast and ovarian cancer (21). Pegylated liposomes, known as sterically stabilized liposomes, are capable of carrying doxorubicin which is one of the most commonly used anthracyclines (18). The use of pegylated liposomal doxorubicin (PLD) offers prolonged circulation time, increase in permeability, and non-toxic circulation (20). PLD enhances therapeutic index with monotherapy and in combination with chemotherapy (20). It has been proven that PLD enhances the therapeutic efficacy with less cardiotoxicity compared to the effect of conventional doxorubicin (19, 22).

Liposomes are non-toxic and biodegradable. This characteristics offer liposomes as a cytotoxic drug and anticancer agent carrier directed to specific tumor site (20). It is crucial to develop nanocarriers such as micelles and liposomes by means of cytotoxic agent carriers with minimal detrimental effect on host cells and maximal drug encapsulation efficiency (20, 23).

1.4. Types of nanocarriers

1.4.1. Polymeric micelles

Micelles are made up of one or two fatty acyl chains self-forming a hydrophobic core-hydrophilic shell structure in an aqueous solution (24). The hydrophobic effect of polymeric micelles allows for fatty acids to aggregate and prevent water molecules from internal core (24). Polymeric micelles, an advanced form of copolymers, have two different chemical properties (25). One is a hydrophobic blocks internal core and the other consists of a dense bush of poly (ethylene oxide) (25). These features of polymeric micelles allow them to be used as a hydrophobic drug carrier (25-28).

The size of polymeric micelles (10-150 nm) increases circulation time (27). The hydrophilic shell can protect loaded drug and sequester and inhibit payload leakage (28). It is also possible that polymeric micelles can be engineered by attaching of fatty acid side group to enhance their encapsulation efficiency (28). Several formulations of micelles have been studied in clinical trials (27). Polymeric micelles have been used to load paclitaxel which is one of the cytotoxic drugs for cancer treatment with conjugation of cancer-specific peptide p160 using the dialysis method (26).

However, there are numerous limiting effects with the use of polymeric micelles from bench to clinic (28). Polymeric micelles as a drug carrier contain low drug encapsulation efficiency, low permeability through the cell membrane, and poor circulation condition (25-28). The engineered micelle shell and the improvement of micelle stability for spatial and temporal drug delivery may be needed to not only overcome these obstacles but also to enhance the therapeutic index of drug delivery carrier (27, 28).

1.4.2. Liposomes

Liposomes have been utilized as drug and gene delivery agents for therapeutic and medical application due to their non-immunogenic, and biodegradable characteristics (23). Liposomes consist of amphipathic phospholipids self-forming into a lipid bilayer surrounding an internal aqueous compartment (23, 29, 30). As shown in Fig 1.3, the hydrophobic core is composed of two esterified fatty acyl chains which are aggregated to each other to form a lipid bilayer (29). The assembled bilayer prevents the diffusion of water-soluble solute across the membrane (24, 29). The head groups, hydrophilic portion of liposomes, strongly interact with water molecules and face outward to form an internal aqueous compartment (24). This characteristic of liposomes allows to carry hydrophilic and hydrophobic therapeutic material such as drugs and genes (30-32). Water-soluble materials can reside in the aqueous core. Liposomes can also contain water-insoluble and lipophilic drug inside the lipid bilayer (30). Liposomes can encapsulate drug, gene and gas either separately or simultaneously (30).

The composition of phospholipids can determine both the degree of bilayer fluidity and the physical properties of the liposomes (24). As depicted in Fig 1.4, Phosphatiylcholine (PC), saturated fatty acids, are less fluid and reside in the exoplasmic face to provide membrane curvature. The cylindrical shape of PC generates a flat monolayer. Phosphatidylethanolamine (PE) contains long tails and a small head group that make corn-shaped lipids. These corn-shaped PE are more fluid and form a curved bilayer. Cholesterol, one of major sterols in animals, plays a key role in cellular membrane. Cholesterol restricts the random movement of long phospholipid tails through an increase in thickness of the bilayer. The curvature of the bilayer is influenced by the polar head groups and non-polar tails of its constituent phospholipids.

The physical properties of liposomes can provide therapeutic applications for targeted delivery with reduced systemic toxicity and minimal premature degradation (33). Several methods have been developed for liposomes to incorporate drug and gene. Liposomes have the

potential to carry small molecular weight drug and short DNA fragment for the treatment of cardiovascular diseases and cancers (30, 32, 34). Tissue plasminogen activator (tPA)-loaded liposomes were used as a targeted drug delivery agent for treatment of thrombolysis (30). Doxorubicin and small molecular weight drugs can be encapsulated into liposomes for cancer therapy (32). Plasmid DNA (pEGFP-N1) encapsulation in liposomes can increase the encapsulation efficiency of DNA to interact with cells (35).

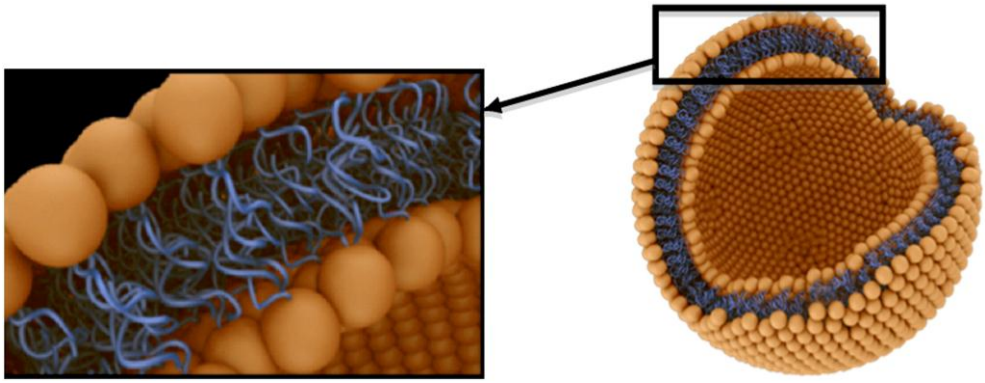

Figure 1.3 Structure of lipids in a bilayer membrane to form liposomes (36)

Permission to Use Granted by Elsevier

Liposomes self-forming into lipid bilayer are clearly separated into hydrophilic region and hydrophobic region. Hydrophilic polar heads are attracted to the water and generate an aqueous core of liposomes. Hydrophobic non-polar tails are directed to each other and form a lipid bilayer.

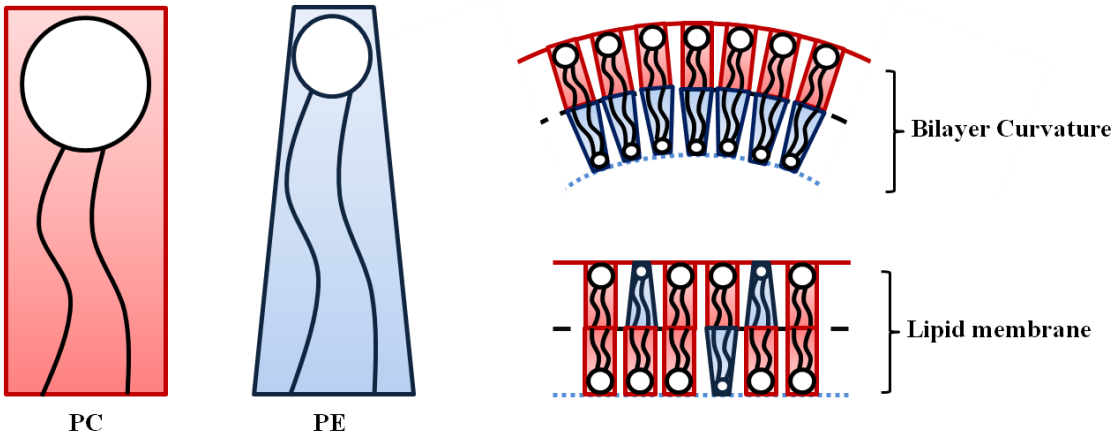

Figure 1.4 Effect of lipid composition on bilayer curvature (24)

Adapted from Lodish, H

The lipid structure of PC is made up of a large hydrophilic head and short hydrophobic tails. However, PE is characterized by a small hydrophilic head and long hydrophobic tails. The interaction between PC and PE generates membrane curved structure. A small hydrophilic head of PE generates better incorporation with inner leaflet. Highly hydrophilic PE resides in exoplasmic face and directs toward water molecule. The mixture of PE and PC forms lipid bilayer.

1.5. Introduction of Echogenic liposomes

1.5.1. Ultrasound contrast agent (UCA)

Ultrasound contrast agent (UCA) refers to particles that reflect and scatter diagnostic ultrasound waves (33). The use of UCA leads to the enhancement of ultrasound images by increasing ultrasonic backscatter (37). The enhancement of backscatter intensity is one of the most crucial factors for the increase of echogenicity for the detection of underlying physiological

features (37, 38). Echogenicity is used for clinical diagnosis of cardiovascular diseases such as thrombus (30, 39).

Echogenic liposomes (ELIP) are developed as a UCA for medical ultrasound imaging and for non-invasive delivery of drugs and genes (33). Ultrasound reflectivity and stability of ELIP can be determined by different lipid formulations and surfactants such as mannitol or BSA, and with varying freezing conditions (40). ELIP formulations have been studied in a multiple number of combinations of phospholipids and cholesterol.

Lipid components of ELIP consist of Egg phosphatidylcholine (EPC), dipalmitoyl-*sn*-glycero-3-phosphocholine (DPPC), dipalmitoyphoshati-dylethanolamine (DPPE), and diapalmitoyl phosphate-dylglycerol (DPPG) with a molar ratio of 27: 42: 8: 8 (41). EPC is unsaturated phospholipids and plays a role in making the lipid a phage region, although it reduces echogenicity (40, 42). Three different saturated phospholipids such as DPPC, DPPG and DPPE participate in the enhancement of ELIP reflectivity. DPPG is negatively charged and facilitates bilayer hydration and prevents liposomes from aggregation (23). Only 8 mole % of DPPG can be used due to toxicity of higher concentration of DPPG (42). Higher concentration of DPPE affects the aggregation of phospholipids. Cholesterol, mostly hydrophobic among the lipid composition, restricts the random movement of phospholipid by increasing the rigidity of lipid bilayer (23, 24).

Mannitol is utilized as a surfactant in ELIP preparation due to its ability to generate ultrasound reflectivity in freeze-thawing cycle (23). The role of mannitol is essential for the disruption of the hydrophobic lipid bilayer which is exposed to air and incorporated with gas (23, 40). Concentration of 0.32 M mannitol can increase the size of liposomes and acoustic stability (40). The optimal concentration of lipid compositions and mannitol solution is crucial for ELIP to be utilized as a UCA to increase ELIP sensitivity to ultrasound application (30).

1.5.2. Gas-containing echogenic liposomes (ELIP)

The amphipathic structure of ELIP provides a design to encapsulate gases allowing direct gas delivery to target tissue (23). ELIP have been developed to contain a wide range of bioactive gases such as argon, nitric oxide, xenon, hydrogen sulfide, and carbon dioxide by elevated pressure with the gas of interest (30).

Several liposomal formulations to incorporate gas and hydrophilic drug into liposomes have been developed by lyophilization and pressurization procedures. (30). Gas-containing ELIP were prepared by the freezing-under-pressure method previously developed in our laboratory (23, 41). After drying and hydrating of the lipid film, liposomes undergo the gas injection process using the elevated pressure-freeze method. Five milligrams of lipids can encapsulate 10 μl of gas using relatively low pressure (23). As shown in Fig 1.5, gas entrapped into ELIP may reside in hydrophobic surface by the difference of surface tension in the amphipathic lipids. Insoluble gas forms a lipid monolayer-covered gas bubble in the aqueous compartment (33).

Gas-containing ELIP have been employed as a UCA for intravascular IVUS images (33). The difference in density between entrapped gas and the lipid dispersion interface can create ultrasound reflectivity and thus high contrast in IVUS images (30). Acoustically active gas-containing ELIP have potential to be visualized in IVUS images in real time (40).

Ultrasound can stimulate release of the payload of ELIP with the interaction with ELIP (37). When gas entrapped into ELIP is exposed to ultrasound, they diffuse from the lipid shell by the expansion of the gas bubbles and the oscillation effect on the liposome's membrane (23, 30). This acoustically active characteristic of gas-containing ELIP allows ultrasound-triggered release of payload as well as ultrasound imaging (40).

The encapsulation of nitric oxide (NO) into ELIP, i.e. NO-ELIP, has the potential to protect NO from being removed by NO scavengers as well as the possibility of liberating NO

from NO-ELIP with ultrasound stimulation (41). The effect of NO-ELIP as a gas delivery carrier has been studied for inhibition of intimal hyperplasia in cardiovascular disease treatment (41). The use of NO-ELIP can provide a tool for a targeted bioactive gas delivery.

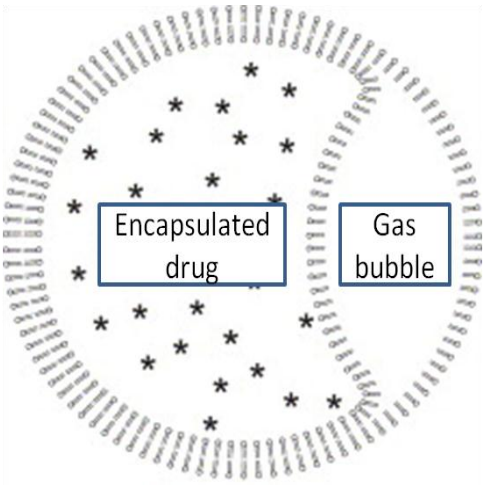

Figure 1.5 Structure of gas-containing ELIP with an internal aqueous phase and a gas bubble between two monolayers (33).

Permission to Use Granted by Elsevier

Two different phages of ELIP allow to encapsulate water-soluble drug into the internal core liposomes and water-insoluble drugs in the bilayer. ELIP can encapsulate gas between two monolayers of lipid hydrophobic face.

1.6. Physiological role of nitric oxide

1.6.1. Role of NO in cancer

Nitric oxide (NO) is a signaling molecule that regulates biological processes through reactions by second messengers (43). The role of NO is highly complex in tumor biology (44). NO has the potential to induce either cancer progression or cancer cell apoptosis depending on intra-tumoral NO concentration (44, 45).

Recent studies have shown that high levels of NO leads to cytotoxic effects on cancer cells by the reaction with O_2^- to generate the formation of peroxynitrite that acts as an apoptosis inducer and toxic species during immune surveillance (46). High levels of NO also results in DNA damage followed by the accumulation of p53 which is a major pro-apoptotic protein and tumor suppressor. The accumulation of p53 meditates release of cytochrome C from mitochondria, also known as intrinsic apoptosis (24).

On the other hand, low level of NO stimulates angiogenesis by the accumulation of vascular endothelial growth factor (VEGF), fibroblast growth factor (FGF) and plate-derived growth factor (PDGF) (44). Cancer cells are able to proliferate the accumulation of VEGF (44, 47). Angiogenesis leads to tumor cell proliferation providing nutrients for growth and is a key factor for tumor cells to metastasize (43).

A number of studies have been recently conducted to identify the use of NO as an onco-preventive agent for cancer treatment (47, 48). The role of NO in tumor biology is associated with the properties and concentration of NO in the tumor microenvironment (44, 46).

1.6.2. NO-induced pathway in breast cancer cells

The role of NO in tumor biology has been studied for more than 40 years, but the dual function of NO for either pro-tumoral or anti-tumoral effect still remains unclear (48). An increasing number of studies has demonstrated that there is a correlation between NO chemistry and cytotoxicity in cancer (46).

The cell cycle, sequence of events for cell proliferation, consists of four phases shown in Fig 1.6 (24). Cell growth is regulated by extracellular growth factor or hormonal signal, mitogen growth factor during G1 phage. The restriction check point is located at G1 phage of the cell cycle, which determines whether the cell grows enough to divide or postpone division or enter a resting stage known as G0. The check point is mainly regulated by the cycline-dependent protein kinase (CDK) inhibitor p16. p16 inhibits activity of cyclin complex, especially CDK 4 and cyclin D1 (49). The down-regulation of cyclin D1 is essential for the inhibition of tumor cell proliferation and tumor regression (49). It has been reported that NO-induced cytotoxicity in cancer is associated with high levels (> 300 nM) of NO. A high levels of NO rapidly develops cytostasis on cancer cells (44).

MDA-MB-231, a highly metastatic and undifferentiated human breast cancer cell, undergoes NO-induced long lasting cytostasis in a high levels of NO (49). Cytostasis refers to a halt in the cell cycle event that results from decreasing the translation of several cell cycle proteins (24). Down-regulation of cyclin D1 prevents retinoblastoma protein (pRb) function which controls the G1-S transition of the cell cycle depicted in Fig 1.6. Hypophosphorylation of pRb induces an inactive E2F transcription factor followed by anti-progression of the cell cycle. This inactive pRb is also known as a tumor suppressor (50).

It has been shown that NO in high concentration leads to MDA-MB-468 cell death through the intrinsic activation with long-term exposure shown in Fig 1.7 (51, 52). The loss of a

fully functional apoptotic program is regarded as the hallmark of all types of tumor cells (50). The mitochondria are known to generate adenosine triphosphate (ATP) for cell respiration and survival and make glucose metabolites (24). However, it has been shown that the mitrochondria participates in apoptosis, known as intrinsic apoptotic pathway, which determines cell life or death. The B-cell lymphoma 2 (BCL-2) protein consists of pro-apoptotic and anti-apoptoic BCL-2 family based on regions of BCL-2 homology (51). The multidomain pro-apoptotic proteins in the large family of BCL-2 family are subgrouped into Bax and Bak family that reside in the outer membrane of mitrochondria (24). The activation of Bax and Bak, integral members of intrinsic apoptosis, is correlated with the interaction between anti- and pro-apoptotic BCL-2 proteins. BH3-only proapoptotic proteins; BIM, BID and PUMA are major upstream regulators of Bax and Bak activity (51). As apoptosis occurs, Bax and Bak trigger the release of cytochrome c and a total collapse of the primary ATP-generating machinery (24). Cytochrome c resides in the intermembrane space of mitochondria and acts as the primary biochemical messenger in apoptotic process (49). After the initiation of apoptosis, the outer membrane of mitochondria becomes depolarized and releases cytochrome c from the mitochondria surface into the cytosol (24). Released cytochrome c activates caspase cascade that activates caspse-9 and other caspases. The levels of BCL-2 family proteins regulate whether cytochrome c is located in the mitochondria or the cytosol.

There are two theories about the role of NO in the intrinsic activation (51). NO promotes the activation of Bax and Bak which results in mitochondrial outer membrane permeabilization (MOMP). This induces cytochrome c spilled out from the intermembrane space to the cytosol followed by activating the caspase-dependent apoptotic signaling cascade (47, 51). Many studies have confirmed that the combined loss of Bax, Bak and caspase-9 activity inhibits NO-induced cell death in MDA-MB-468 cells (51, 52). NO-induced activation of intrinsic apoptotic pathway induces programmed cell death in MDA-MB-468.

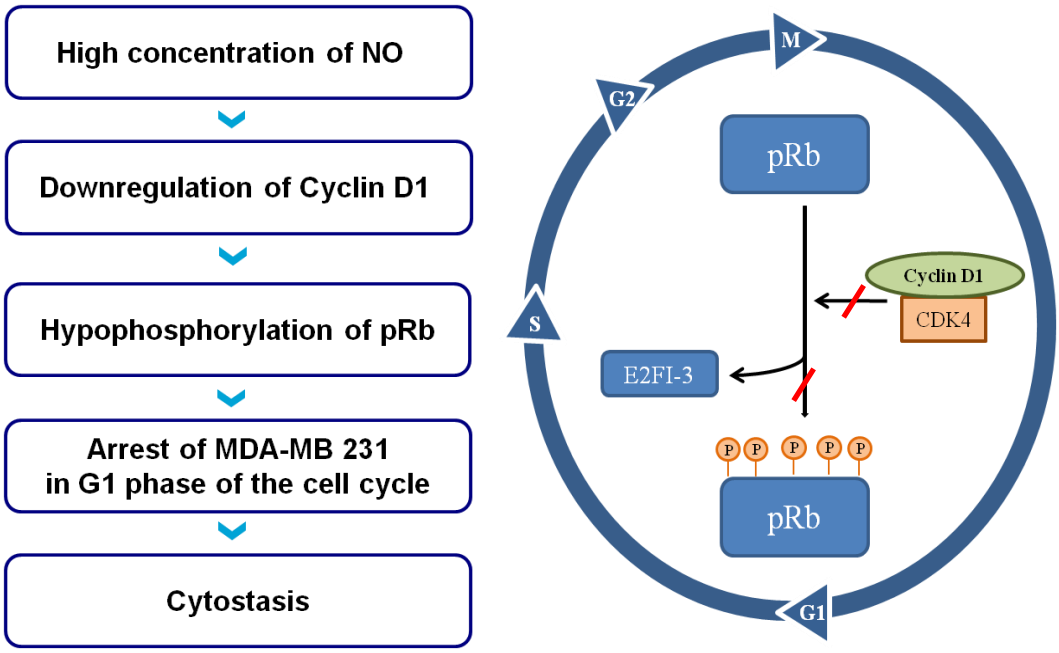

Figure 1.6 NO-induced cytostasis in MDA-MB-231 (24)

Adapted from Lodish, H

MDA-MB-231 exposed to high concentration of NO is arrested at G1 phase of the cell cycle. Cyclin D1 and CDK4 complex plays a key role to transition from G1 to S phase of the cell cycle. NO-induced down- regulation of cyclin D1 inactivates pRb phosphorylation which activates E2F1-3 transcription factor to generate cyclin/CDK complex for entering S phage of the cell cycle. The down- regulation of cyclin D1 can induce NO-induced long lasting cytostasis.

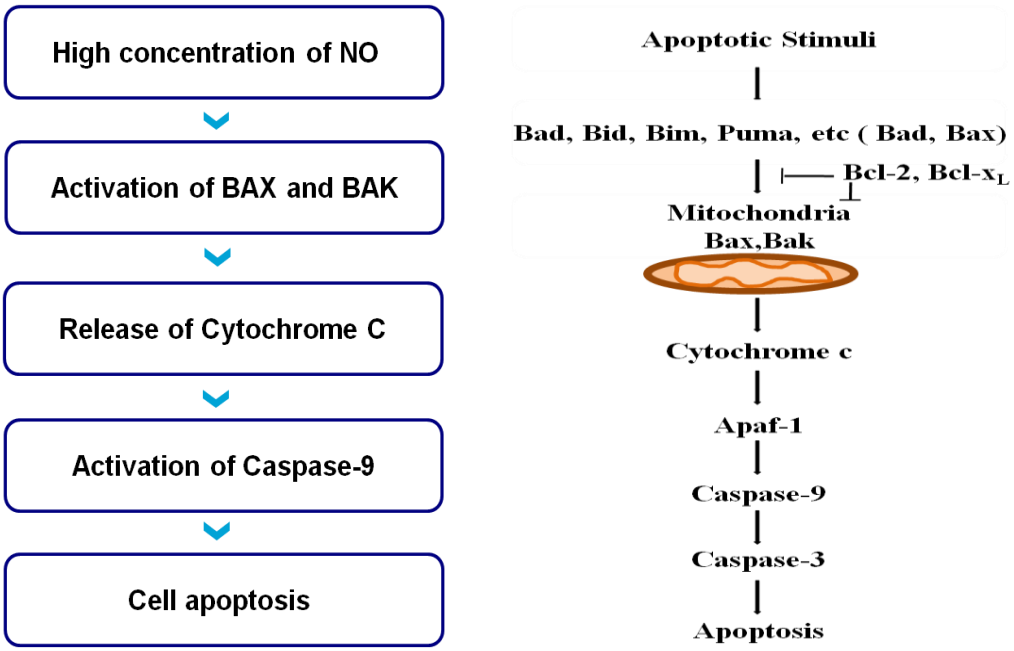

Figure 1.7 NO-induced apoptosis in MDA-MB-468 (24)

Adapted from Lodish, H

High levels of NO induce the intrinsic apoptotic pathway in MDA-MB-468 cell. NO activates Bax and Bak proteins to release cytochrome C from mitochondria. Cytochrome C activates caspase cascade followed by inducing cell apoptosis.

CHAPTER 2

Specific Aim 1 - Development of NO-ELIP for Breast Cancer Treatment

2.1. Materials and methodologies

2.1.1. NO-ELIP preparation by the freezing-under-pressure method

NO-ELIP was prepared by the previously developed freezing-under-pressure method with the modification of lipid composition (41). All phospholipids and cholesterol were purchased from Avanti Polar Lipids (Albaster, AL, USA). Echogenic liposomal dispersion consists of Egg L-α-phosphatidylcholine (EPC); 1,2-dipamitoyl-s*n*-glycero-3-phosphocholine (DPPC), L-α-dipalmitoylphosphatidyl-ethanolamine (DPPE), 1,2-diapalmitoyl-*sn*-glycero-3-[phosphor-rac-l-glycerol] (DPPG) and 3β-[N-(N',N'-dimethylaminoehane)-carbamoyl] cholesterol hydrochloride (DC-Cholesterol·HCl) with a molar ratio of 27:42:8:8:15. The molar percentage of saturated lipid was previously studied to increase the retention of echogenic stability. The saturated phospholipid, DPPC is essential for the lipid formulation to increase echogenicity. The stability of echogenicity of NO-ELIP was maximized at the amount of 42 mole % DPPC. The use of DC-Cholesterol·HCl, positively charged lipids, generates a cationic polar head group of liposomes. The surface of positively charged liposomes improves the interaction with negatively charged BCC membrane. The optimal concentration of cholesterol was determined to be 15 mole % to maximize the acoustic stability of NO-ELIP and generate substantial response with BCC.

Four phospholipids and cholesterol hydrochloride were dissolved in organic solvent (chloroform and methanol at 9:1 ratio) to obtain lipid solution. The lipid solution underwent dry process to form a thin lipid film using argon in a 50 ℃ H_2O bath. Remaining organic solvent was completely removed by high vacuum at ≤ 100 mTorr overnight. The lipid film was placed under ultraviolet (UV) light for 15 minutes for sterilization. The hydration of the lipid film was performed with deoxygenated 0.32 M mannitol. The final concentration of liposomal dispersion was 10 mg/ml. Liposomal dispersion was sonicated for 5 minutes in a bath sonicator. The sonicated liposomal dispersion was transferred into a 1.8 ml screw-cap borosilicate glass vial. It

is essential to keep the hypoxic condition in solution to reduce NO reaction with oxygen. Nine milliliters of NO washed and deoxygenated using the crystal form of sodium hydroxide (NaOH) was injected into the glass vial through the use of a 12 ml syringe with a 0.5″ needle applying elevated pressure. Liposomal dispersion containing NO, known as NO-ELIP, was incubated for 30 minutes at room temperature. Pressurized liposomes were placed in -80 ℃ freezer for overnight.

2.1.2. Measurement of echogenicity using intravascular ultrasound

Echogenicity of NO-ELIP was measured with the use of a 20-MHz high-frequency intravascular ultrasound (IVUS) imaging catheter. NO-ELIP, resuspended in 5 ml of phosphate buffered saline (PBS) in a 12×16 glass vial, was diluted to a concentration 0.1 mg/ml for IVUS imaging. The catheter was inserted into the glass vial containing 50 μl of resuspended NO-ELIP in 5 ml of PBS. The retention of ultrasound reflectivity of NO-ELIP was determined by measuring the mean gray scale value (MGSV) in a region of interest (ROI) in the IVUS image. MGSV of NO-ELIP resuspended in 10 mg/ml of BSA in PBS (PBS/BSA) was measured every 10 minutes until the first hour, and then once per hour up to 5 hours. Images of diluted NO-ELIP were recorded in real time for subsequent playback and image analysis. Ultrasound images were digitized with 8-bit (256 gray level) 640×480 pixel spatial resolution. As shown in Fig 2.1, the region of interest was manually traced between the vial wall and the imaging catheter to calculate MGSV of NO-ELIP excluding the area of the strut artifact of the IVUS images catheter. MGSVs in the ROI were quantitated using Image-Pro Plus software (Version 4.1, Media Cynernetics, Silver Spring, MD).

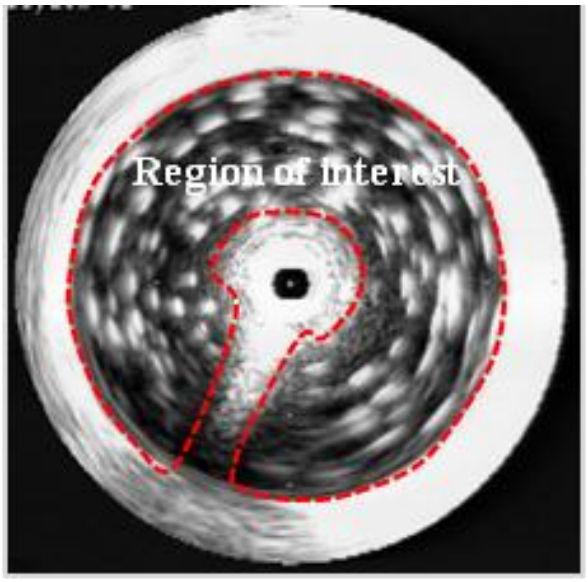

Figure 2.1 IVUS image of a glass vial containing NO-ELIP

Outer ring indicates the glass vial containing 0.1 mg/ml of NO-ELIP. The black dot in the center of the IVUS image represents the catheter. The red line between the glass vial wall and catheter indicates ultrasound responsive liposomes. This area was set as an ROI. The brightness in the ROI was quantitated as a MGSV.

2.1.3. BCC lines and cell culture conditions

Two BCC lines, MDA-MB-231 and MDA-MB-468 from the America type culture collection, (ATCC, VA, USA), were obtained from Dr. Sharina's laboratory in the Division of Cardiology at the University of Texas Health Science Center at Houston (UT-HSCH). These BCC lines respond differently to high level of NO with the induction of different cellular pathways. MDA-MB-231 is a highly undifferentiated BCC line with the absence of endogenous NO production (49). This cell line was originally isolated from an aneuploid female with mammary gland ductal carcinoma. On the other hand, MDA-MB-468 was isolated from a 51-year-old female patient with metastatic adenocarcinoma of the breast and has relatively high arginase activity which is a common substrate from L-Arginine (52).

The BCC lines were maintained with Dulbeccos's modified Eagle Medium (DMEM-High Glucose) supplemented with 10% fetal bovine serum (FBS), 5% penicillin streptomycin, 5% 100 mM sodium pyrurate, 5% MEM non-essential amino acids, 5% 1M HEPES at a temperature of 37 ℃ in 0.5% of CO_2.

2.1.4. Identification of BCC growth rate

It is important to determine the growth rate of BCCs to optimize breast cancer cell culture conditions and estimate the cell cycle of each BCC line. The number of BCCs was counted at different time points (0, 12, 24, and 48 hours) using a hemacytometer. The use of this hemacytometer evaluates the number of cells per unit volume of a cell suspension by counting cells under microscope. The instrument consists of a glass cover slip, counting chambers and a sample introduction point. After the trypsinization of BCCs, uniform suspension of cells was diluted to avoid overlapping of cells in the counting chamber. Ten microliters of cell suspension was introduced at the edge of v-shape of the chamber per slide. The hemacytometer was placed

on the microscope stage at 100 times magnification and cells above four 1 mm^2 areas of the counting chamber were counted. The total number of cells was calculated as follows.

$$\left(\frac{\text{The number of cells counted} \times \text{Dilution factor} \times 10^4}{\text{The number of squared counted}}\right) \times \text{total volume of suspension (ml)}$$

2.1.5. Determination of BCC density

3-(4, 5-dimethylthiazol-2-yl)-2-5diphenyltetrazolium bromide (MTT) viability assay was utilized for quantitative identification of cellular proliferation with response to growth factor and cytokines. BCCs were plated into a 96 well plate with a final volume of 100 µl. Cell suspension was diluted using 1:2 dilution in order to find optimal cell density for MTT assay. Thiazoly blue tetrazolium bromide dissolved in PBS was prepared as a MTT solution. BCCs were incubated with 10 µl of MTT solution (5 mg/ml in PBS) for 2 hours at 37 ℃ in 0.5 % of CO_2. The MTT solution was allowed to be metabolized and the cleavage of formazan dye recorded by spectrophotometer. Resuspended formazan in 100 µl Dimethylsulfoxide (DMSO) was utilized to read optical density at 580 nm using a SpectraMax® M5 spectrophotometer (Molecular Devices, California, USA), to determine a correlation with cell quantity.

2.2. Results

2.2.1. Stability of echogenicity of NO-ELIP

As depicted in Fig 2.2, MGSVs of NO-ELIP resuspended in PBS/BSA decreased over time. NO-ELIP resuspended in PBS/BSA showed high echogenicity with MGSV of 174 ± 17 at 0 minute. While there was a stiff decrease of echogenicity until 60 minutes, the rate of echogenicity reduced afterwards. MGSV of NO-ELIP with PBS/BSA reduced to 60 ± 2 in an hour. NO-ELIP retained echogenicity with MGSV of 30 ± 12 at 5 hours.

NO-ELIP resuspended in PBS lost echogenicity over time as shown in Fig 2.3. There was a rapid decrease of echogenicity in the first hour with MGSV of 13 ± 5 and the echogenicity disappeared at 3 hours. The stability of NO-ELIP in PBS lasted for 3 hours.

Fig 2.4 shows the combined data of the echogenicity of NO-ELIP resuspended in PBS and in PBS/BSA. There was a 40% enhancement of echogenicity of NO-ELIP in the presence of PBS/BSA as compared to that in PBS at 1 hour ($p < 0.01$). Echogenicity of NO-ELIP resuspended in PBS disappeared within 3 hours, yet that in BSA remained their echogenicity up to 5 hours. Echogenicity of NO-ELIP resuspended in BSA/PBS was different from that in PBS ($p < 0.05$).

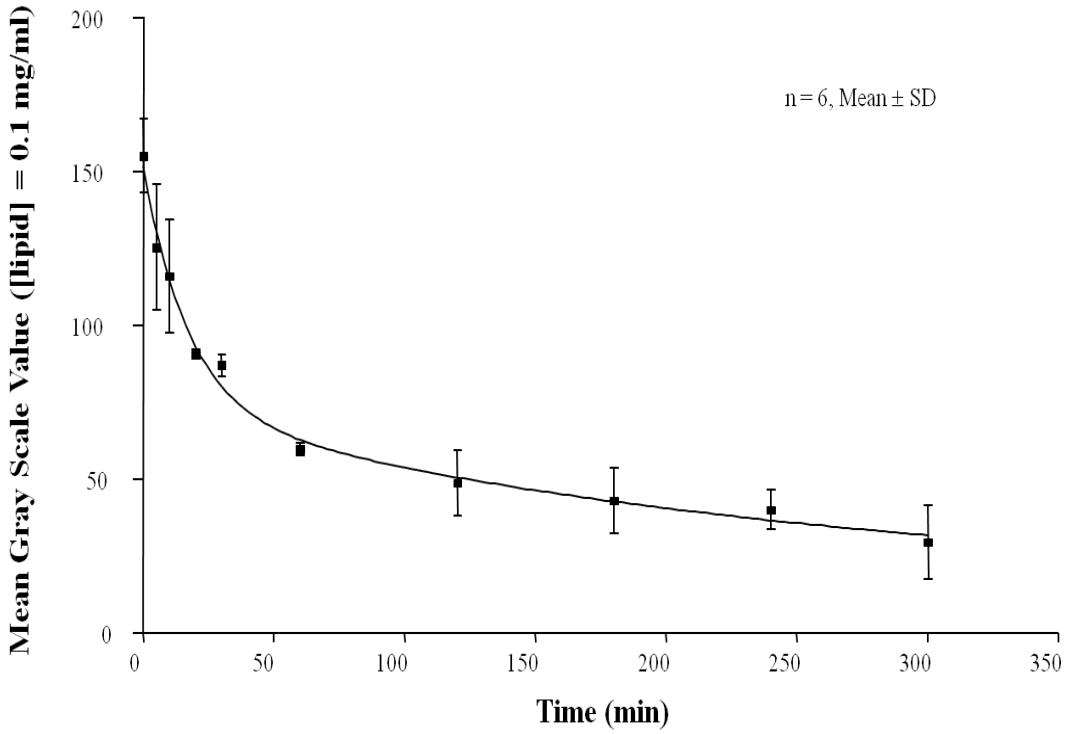

Figure 2.2 Echogenicity of NO-ELIP resuspended in PBS/BSA

The graph depicts the stability of NO-ELIP in PBS/BSA up to 5 hours. MGSVs of NO-ELIP resuspended in PBS/BSA were measured up to 5 hours. NO-ELIP were diluted to 0.1 mg/ml in 10 mg/ml of BSA containing PBS.

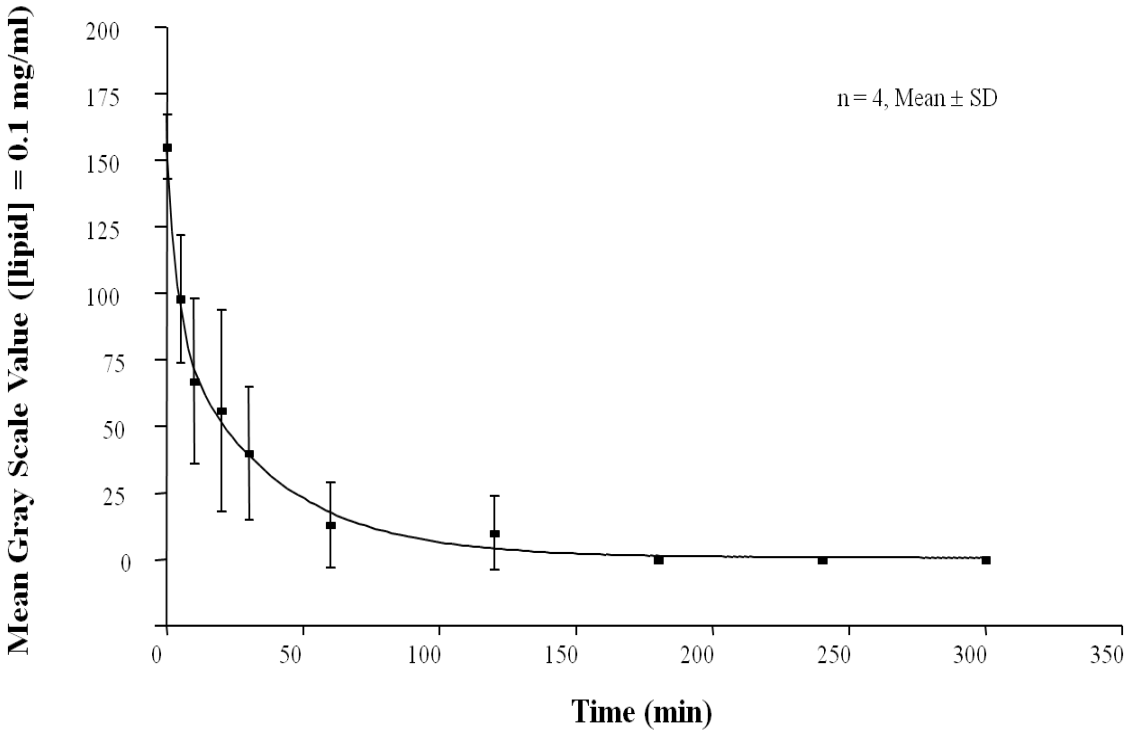

Figure 2.3 Echogenicity of NO-ELIP resuspended in PBS

The graph depicts the stability of NO-ELIP in PBS up to 5 hours. MGSV2 of NO-ELIP resuspended in PBS was measured up to 5 hours using IVUS images. NO-ELIP were diluted to 0.1 mg/ml in PBS.

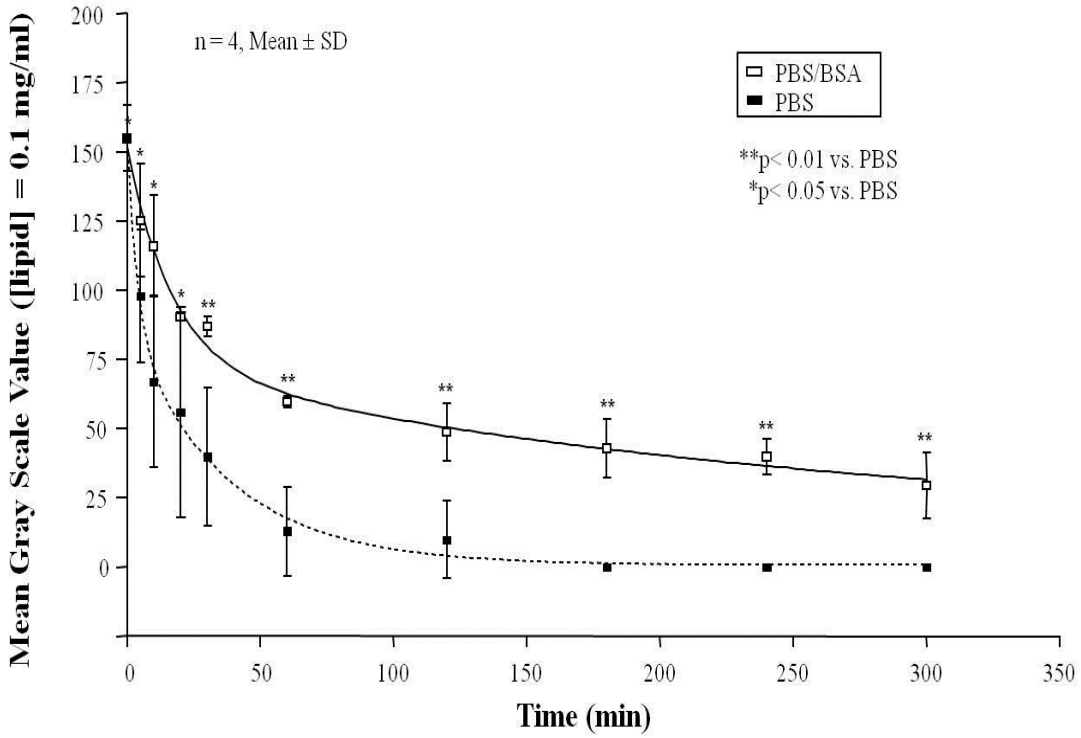

Figure 2.4 Echogenicity of NO-ELIP resuspended in PBS/BSA and in PBS

The top line indicates MGSV of NO-ELIP resuspended in PBS/BSA. The bottom line represents MGSV of NO-ELIP resuspended in PBS. Echogenicity of NO-ELIP suspended in PBS/BSA was different from that in PBS ($p < 0.05$).

2.2.2. Identification of growth rate and density of BCC

The growth rate and cell density of BCC were evaluated to optimize culture conditions. As shown in Fig 2.5, the doubling time of MDA-MB-231 cells was found to be 24 hours in the middle of the exponential growth phase. On the other hand, the number of MDA-MB-468 cell became almost doubled after 36 hours as depicted in Fig 2.6. The growth rate of MDA-MB-468 was slower than that of MDA-MB-231.

As depicted in Fig 2.7, MDA-MB-231 cell concentration was measured by optical density evaluated by the turbidity of cell suspension to estimate cell density. Optimal cell densities of MDA-MB-231 cells were determined in the linear range of detection. Five hundred thousands cells/ml of MDA-MB-231 were seeded in a 96 well plate at approximately 80 % of cell confluency. As shown in Fig 2.8, optimal concentration of MDA-MB-468 cells was also 5×10^5 cells/well in linear range of detection. These cell concentrations were used for subsequent MTT assay studies.

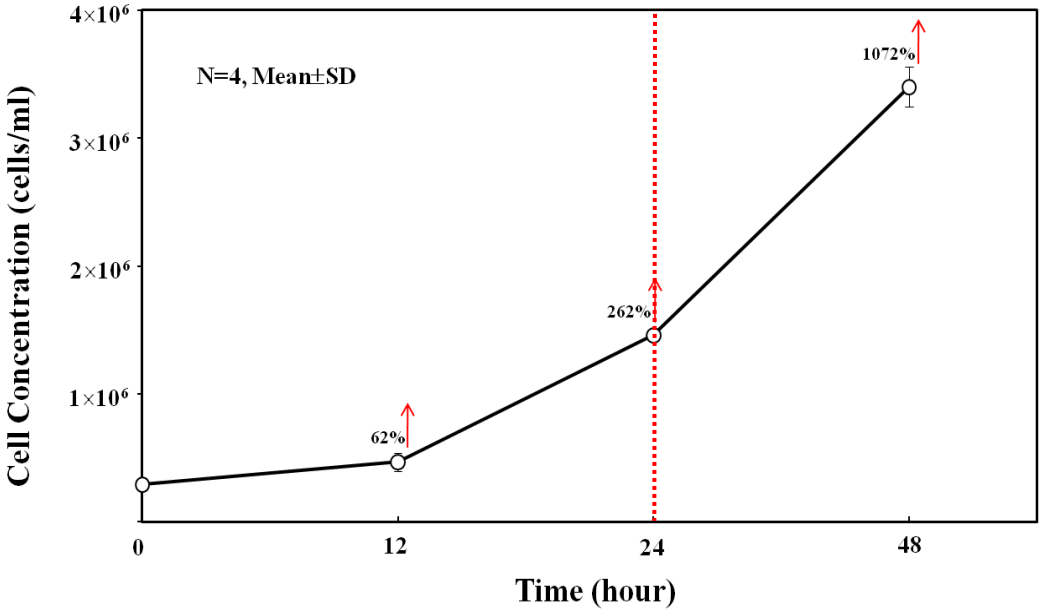

Figure 2.5 MDA-MB-231 growth curve

MDA-MB-231 cell growth rate was determined by counting the number of cells from 12 hours up to 48 hours. Results are shown as mean and standard deviation of MDA-MB-231 cell concentrations from four independent experiments.

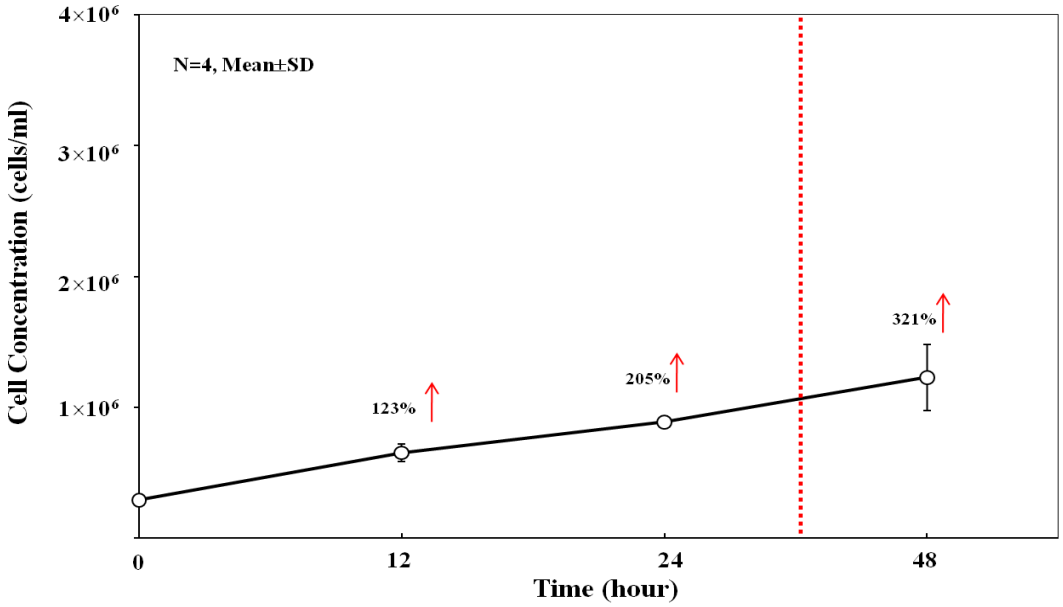

Figure 2.6 MDA-MB-468 growth curve

MDA-MB-468 cell growth rate was measured by counting the cell number from 12 hours to 48 hours. Results are expressed as the mean and standard deviation of MDA-MB-468 cell concentrations from four different experiments.

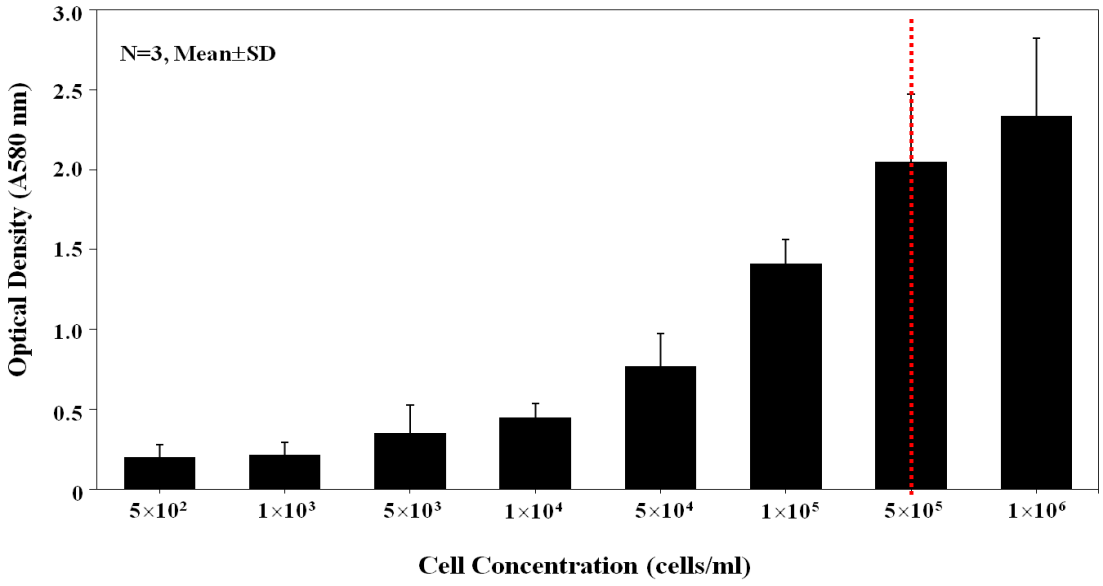

Figure 2.7 MDA-MB-231 cell densities

Various cell concentrations of MDA-MB-231 cell were seeded into 96 well plate to determine optical density for MTT assay. Optical density increased as MDA-MB-231 cell concentration increased. Red line indicates the optimal density (5×10^5 cells/ml) of MDA-MB-231 determined in the linear range of detection for MTT assay.

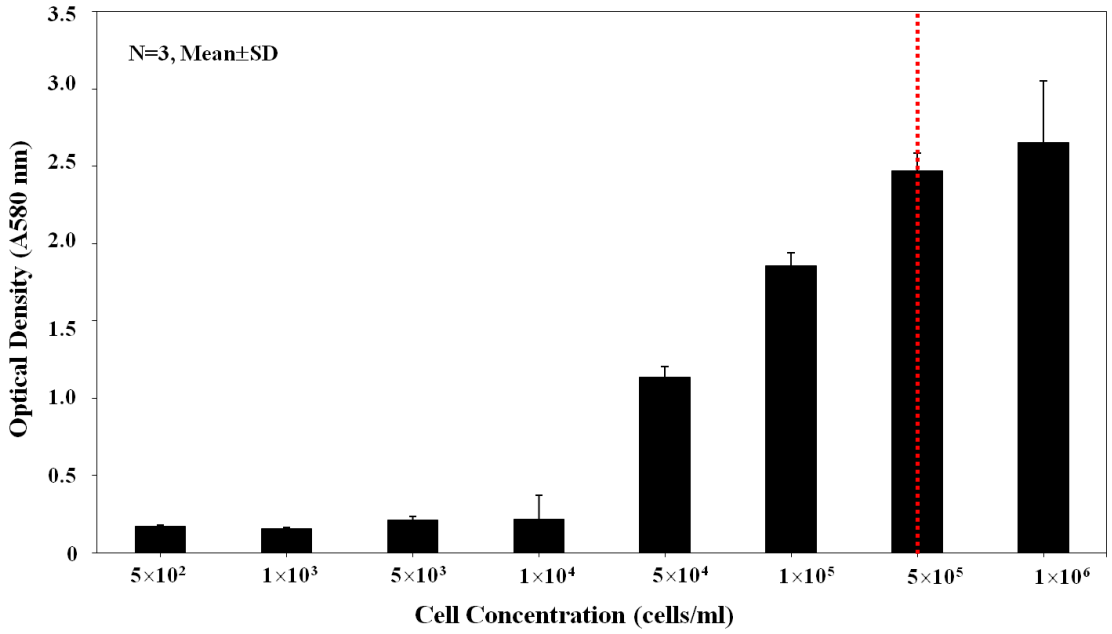

Figure 2.8 MDA-MB-468 cell densities

Various cell concentrations of MDA-MB-468 cell were seeded into 96 well plate to determine optical density for MTT assay. Optical density increased as MDA-MB-468 cell concentration increased. Red line indicates the optimal density (5×10^5 cells/ml) of MDA-MB-468 determined in the linear range of detection for MTT assay.

2.3. Discussion

The primary objective was to determine liposomal formulation of NO-ELIP for breast cancer treatment. NO-ELIP was prepared by the freezing-under-pressure method as described. The stability of NO-ELIP was evaluated by measuring of MGSVs in a region of interest in IVUS images. The condition of breast cancer cell culture was optimized by measuring of growth rates using hemacytometer and optimal cell densities using MTT viability assay.

The lipid formulation was previously identified as EPC: DPPC: DPPE: DPPG: DC-cholesterol·HCl, with a molar ratio of 27:42: 8: 8: 15 (42). The use of 0.32 M mannitol improved ultrasound reflectivity of NO-ELIP indicating that lipid fusion to incorporate gas of interest occurred during the freezing process (30). The addition of DC-Cholesterol·HCl in NO-ELIP preparation generated positively charged NO-ELIP and preserved lipid bilayer structure.

The stability of NO-ELIP was evaluated by the measurement of echogenicity over time. Previous studies in our laboratory have shown that NO gas entrapped in the lipid bilayer of ELIP has the potential to generate ultrasound reflectivity and to be visualized in IVUS images (23, 30). Fifty percent of NO resuspended in PBS/BSA was released from NO-ELIP in 1 hour and 24 % of NO slowly diffused up to 5 hours. On the other hand, NO-ELIP resuspended in PBS released 50 % of NO in 20 minutes and 96 % of NO diffused out of NO-ELIP by 1 hour. The results indicate that the use of BSA for resuspension of NO-ELIP can provide a more stable environment. The surface of positively charged NO-ELIP interacted with the anionically charged BSA molecule following the coating effect produced by BSA molecule on the surface of ELIP (30). The BSA-coated NO-ELIP may prevent gas leakages and stiffen the lipid structure.

BCC doubling time is described by plotting a growth curve at various time points throughout the growth cycle. Time-dependent BCC growth rate is crucial for the optimization of BCC culture conditions in-vitro and the quantification of different treatment modalities (2).

BCCs enter exponential growth during which the cell population doubles over a definable period and characteristic for each BCC lines. MDA-MB-231 cell population became doubled at 24 hours allowing the cells to recover from trypsinization, construct their cytoskeleton and enable them to re-enter the cell cycle. Population doubling of MDA-MB-468 was at approximately 36 hours. The determination of doubling time of BCCs provides the consistency of experimental condition for BCC preparation.

Cell densities imply that the cells are attached and affect cell proliferation and differentiation (6). At a high level of cell density, there is limited nutrient perfusion and limited incidence of apoptosis in differentiated cells. On the other hand, low cell density is prone to induce nutrient deprivation and induces the absence of cell contact signaling. It is crucial to identify optimal cell density of BCC lines to conduct MTT assay. Optical density measurement is important to convert into BCC viability in MTT assay. Therefore, a strong signal on optical density within the linear range of detection is required to determine BCC viability. Five hundred thousand cells per ml were determined as the optimal cell density for both BCC lines.

CHAPTER 3

Specific Aim 2 – Efficiency of NO Delivery Strategy Using NO-ELIP

3.1. Materials and methodologies

3.1.1. NO-donor treatment for BCC lines

MDA-MB-231 cells were seeded into a 96 well plate at a density of 5×10^5 cells/well in 100 µl. After 24 hours, the cells reached approximately 80% of cell confluent. They were serum-starved overnight and washed once with PBS. The stock solution of Spermine-NONOate was 1mM. A serial dilution using a dilution factor of 3 was performed with 0.1 M solution of NaOH. Synchronized cells were exposed to 100 µl of the mixture of 4.1 µl of Spermine-NONOate and 410 µl of serum free medium, and placed at 37 ℃ and 0.5 % of CO_2 for 24 hours.

MDA-MB-468 cells were plated into a 96 well plate at a density of 5×10^5 cells/well in 100 µl. After 36 hours, the cells were serum-starved overnight and washed once with PBS. DETA-NONOate in 1 mM was diluted by a factor of 3. One hundred microliters of the mixture of 4.1 µl of DETA-NONOate and 410 µl of serum free medium were treated to synchronize MDA-MB-468 cells. The cells were exposed to DETA-NONOate for 24 hours at 37 ℃ and 0.5 % of CO_2.

MTT viability assay was performed introducing 10 µl of MTT solution 5 mg/ml in PBS into each well for 2 hours. One hundred microliters of solubilization solutions were added into each well and incubated for an hour at 37 ℃ and 0.5 % of CO_2. Purple formazan crystal was completely solubilized, which allowed the quantitation of absorbance of purple formazan crystal at 570 nm using SpectraMax® M5 spectrophotometer (Molecular Devices, CA, USA).

3.1.2. NO-ELIP treatment for BCC lines

3.1.2.1. Effect of NO-ELIP on BCCs in PBS

Breast cancer cells, MDA-MB-231 cells and MDA-MB-468 cells were prepared in a 48 well plate at a density of 5×10^5 cells/well and allowed to grow depending on their growth rate. After reaching 80 % of cell confluence, BCCs underwent serum starvation overnight and was washed once with PBS. PBS underwent a degassing process using a vacuum machine followed by the introduction of 30 ml of argon gas. Degassed PBS was sterilized using 0.45 µm of filter (Millipore, Co Cork, Ireland). BCCs were treated with a serial dilution of NO-ELIP using a dilution factor of 2 resuspended in degassed PBS. BCCs were exposure to 100 µl of NO-ELIP with 400 µl of base medium at 37 ℃ and 0.5 % of CO_2 for 5 hours. After 5 hours, BCCs were washed twice with PBS. An MTT viability assay was performed. The yellow MTT solution was made up of 5 mg of thiazoly blue tetrazolium bromide in 1 ml of PBS which allowed a final concentration of 5 mg/ml. BCCs were incubated with 10 µl of MTT solution at 37 ℃ and 0.5 % of CO_2 for 2 hours. One hundred microliters of DMSO was introduced into each well. Optical density was measured at 570 nm using SpectraMax® M5 spectrophotometer (Molecular Devices, California, USA).

3.1.2.2. Effect of NO-ELIP on BCCs in BSA

BCCs were plated in a 48 well plate at a density of 5×10^5 cells/well and allowed to grow depending on their growth rate. They underwent serum starvation overnight and were washed once with PBS. Ten milligrams of BSA was added into 1 ml of degassed PBS which had been filtered 0.45 µm for sterilization. NO-ELIP underwent serial dilutions of 1, 0.9, 0.5, 0.25, and 0.125 mg/ml with filtered PBS/BSA. BCCs were treated with 100 µl of NO-ELIP and 400 µl of medium and placed in an incubator 37 ℃ and 0.5 % of CO_2 for 5 hours**.** An MTT viability

assay was performed after the treatment with NO-ELIP in order to determine BCC viability. The yellow MTT solution was made up of 5 mg of thiazoly blue tetrazolium bromide in 1 ml of PBS. BCCs were incubated with 10 μl of MTT solution at 37 ℃ and 0.5 % of CO_2 for 2 hours. One hundred microliters of DMSO was introduced into each well and optical density was measured at 570 nm using SpectraMax® M5 spectrophotometer (Molecular Devices, CA, USA).

3.1.3. Data analysis

Optical density obtained from the MTT assay was transformed to a percentage of cell viability with respect to a control with no treatment. The lowest measured value of cell viability, as a baseline response, was subtracted from all other data. The highest measured value was regarded as 100% allowing all data to be normalized to the 100% scale.

Dose response curves were determined by nonlinear regression curve fitting using the equation of $Y = \frac{100}{1+10^{(X-\log IC_{50})}}$ with the slope factor. This method can provide regression and outlier removal. A sigmoidal dose response curve was generated that follows Gaussian or normal distribution function (Graphpad Prism 3.0, GraphPad Software Inc, CA, USA).

IC_{50}, known as a half-maximal inhibitory concentration, is the concentration of a cytotoxic agent to induce approximately 50 % decrease of cell viability (53). IC_{50} is also defined as the concentration to generate a half way response between the baseline and maximal response (53). The IC_{50} values of the NO-donors were obtained in logarithmic scale as a log IC_{50}. The anti-logarithm of IC_{50} is required to convert to the concentration of NO-donors. For example, NO-donor concentration were 1, 3, 10, 30, 100, 300, 1,000, 3,000, and 10,000 μM and converted to logarithmic scale; 0.0, 0.5, 1.0, 1.5, 2.0, 2.5, 3.0, 3.5, and 4.0. However, it was not necessary to transform the concentrations of NO-ELIP to logarithmic scale due to the short range order in concentration.

3.2. Results

3.2.1. NO-dose dependent MDA-MB-231 cell viability by spermine-NONOate treatment

Dose response curves for MDA-MB-231 cell viability with spermine-NONOate treatment are depicted in Fig 3.1. Each point is presented with mean ± standard deviation for 14 samples. IC_{50} values ranged from 0 to 4 log μM of Spermine-NONOate (corresponds from 1 to 10,000 μM). Spermine-NONOate with concentration ranged from 0 to 2 μM in a logarithmic scale (corresponds from 1 to 30 μM) showed little cytotoxicity on MDA-MB-231 cell viability. The IC_{50} value in MDA-MB-231 was 2.82 μM in a logarithmic scale (corresponds to 656 μM). This result indicates that MDA-MB-231 responded to Spermine-NONOate in a dose-dependent manner and approximately 50% inhibition of MDA-MB-231 cell viability was induced from 656 μM spermine-NONOate.

3.2.2. NO-dose dependent MDA-MB-468 cell viability by DETA-NONOate treatment

The cytotoxic effect of DETA-NONOate on MDA-MB-468 cell viability was examined as illustrated in Fig 3.2. Data shown are as mean ± standard deviation with 14 samples. DETA-NONOate with concentration ranged from 0.47 to 2 μM in a logarithmic scale (corresponds from 3 to 100 μM) had little effect on MDA-MB-468 cell death. The IC_{50} value of DETA-NONOate was 2.59 μM on a logarithmic scale (which is equal to 397 μM). DETA-NONOate in 397 μM concentration induced 50% inhibition of MDA-MB-468 cell viability. Higher concentration of DETA-NONOate over the IC_{50} potentiated to induce maximal cytotoxicity on MDA-MB-468 cell viability.

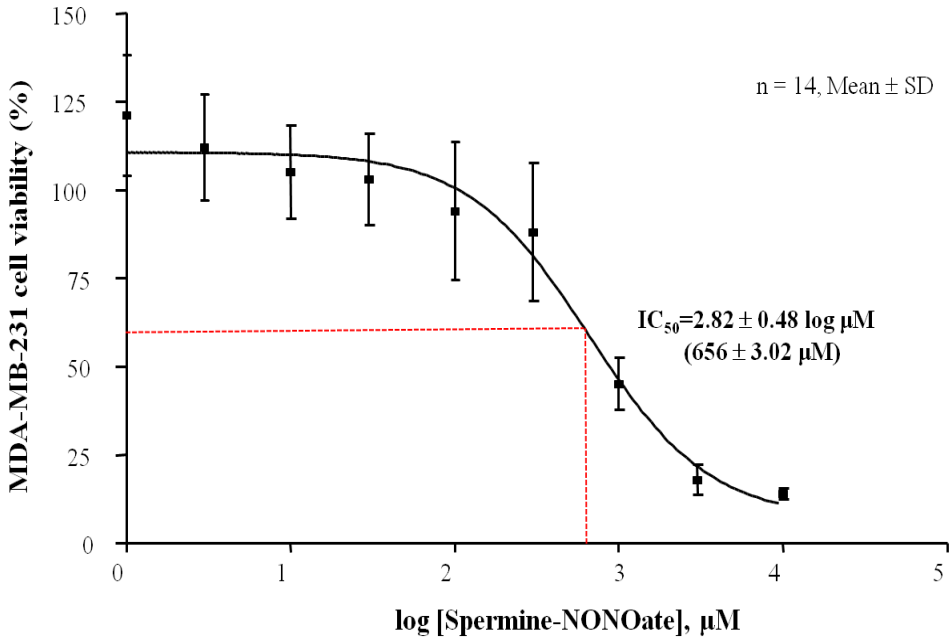

Figure 3.1 MDA-MB-231 cell viability with Spermine-NONOate

MDA-MB-231 cell viability was determined by MTT assay. Data are shown as mean ± standard deviation from fourteen independent experiments. The dose response curve was obtained. IC_{50} value of Spermine-NONOate was 656 ± 3.02 µM.

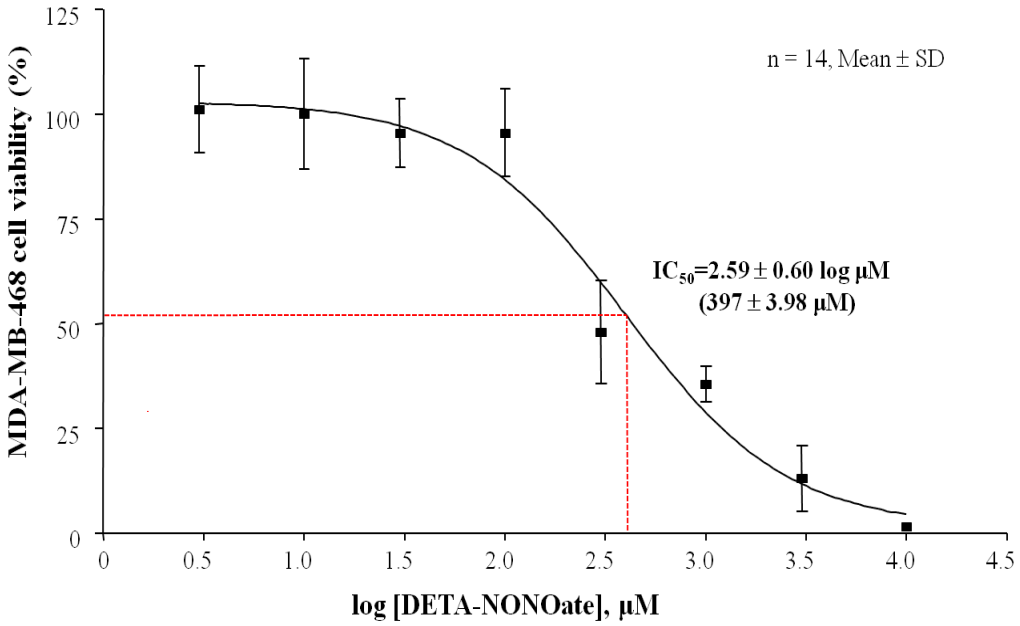

Figure 3.2 MDA-MB-468 cell viability with DETA-NONOate

MDA-MB-468 cell viability was determined by MTT assay. Results are shown as mean ± standard deviation from fourteen independent experiments. The dose-response curve was obtained. IC_{50} value of DETA-NONOate was 397 ±3.98 µM.

3.2.3. Dose dependent BCC response to NO-ELIP resuspended in PBS

To confirm NO-induced cell death and lipid effect on BCCs, NO-saturated mannitol and empty ELIP were treated to BCCs. As shown in Fig 3.3, only 1 % MDA-MB-231 cells were alive with NO-saturated mannitol. On the other hand, 85 % MDA-MB-231 cells remained viable with 1 mg/ml of empty ELIP. Sixteen percent of MDA-MB-468 cells were alive with NO-saturated mannitol as depicted in Fig 3.4. There was 77 % MDA-MB-468 viability after treated with 1 mg/ml of empty ELIP. The results represent that NO-induced cytotoxicity is not from lipid toxicity but mainly due to the NO-saturated mannitol.

NO-ELIP induced concentration-dependent cytotoxic effect on MDA-MB-231 is depicted in Fig 3.5. NO-ELIP in concentrations of 0.125 and 0.25 mg/ml generated little cytotoxicity on MDA-MB-231. The NO-ELIP concentration of 0.7 mg/ml was determined to be the cytotoxic IC_{50} at which MDA-MB-231 cell growth was inhibited to around 50 %. There was only 1 % of MDA-MB-231 cells remained alive with 1 and 2 mg/ml of NO-ELIP. The concentration of NO-ELIP over 1 mg /ml was effective to induce maximum cytotoxic activity on MDA-MB-231 cells. This result indicates that MDA-MB-231 cells respond to NO-ELIP depending on concentration, and 0.7 mg/ml of NO-ELIP is the critical concentration to inhibit 50% of MDA-MB-231 cell growth.

The concentration response curve on MDA-MB-468 is shown in Fig 3.6. NO-ELIP in concentrations of 0.125 and 0.25 mg/ml induced in high MDA-MB-468 cell viability. The cytotoxic IC_{50} value of NO-ELIP inhibiting MDA-MB-468 cell growth by approximately 50 % was 0.47 mg/ml. The concentration of NO-ELIP over 0.7 mg/ml can effectively induce MDA-MB-468 cell death. The data indicates a dose-dependent relationship between NO-ELIP concentration and MDA-MB-468 cell response. NO-ELIP in concentration of 0.47 mg/ml has potential to be used as the critical concentration of NO-ELIP to induce approximately 50 % of MDA-MB-468 cell death.

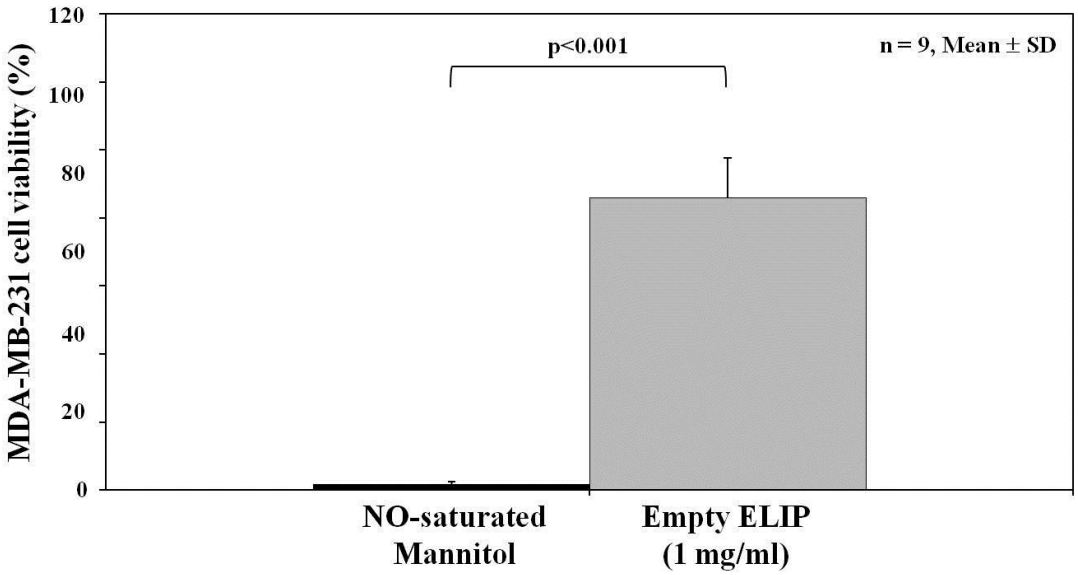

Figure 3.3 MDA-MB-231 cell viability with NO-saturated mannitol and empty ELIP

MDA-MB-231 cell viability was determined by MTT assay. Data are shown as mean ± standard deviation from nine different experiments. These results demonstrated a difference between the two groups ($p < 0.001$).

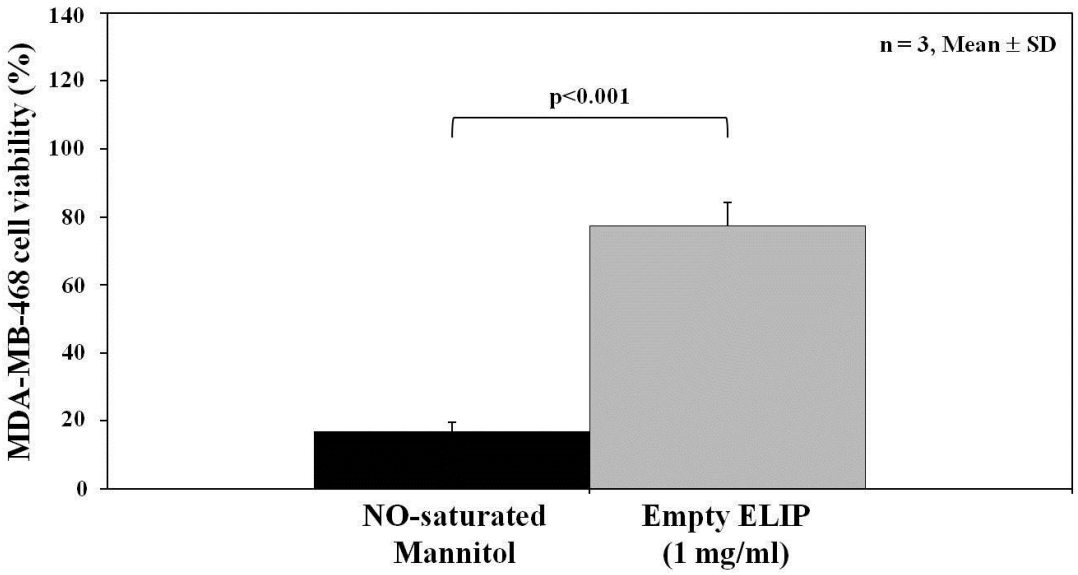

Figure 3.4 MDA-MB-468 cell viability with NO-saturated mannitol and empty ELIP

MDA-MB-468 cell viability was determined by MTT assay. Data are shown as mean ± standard deviation from three different experiments. These results demonstrated a difference between the two groups ($p < 0.001$).

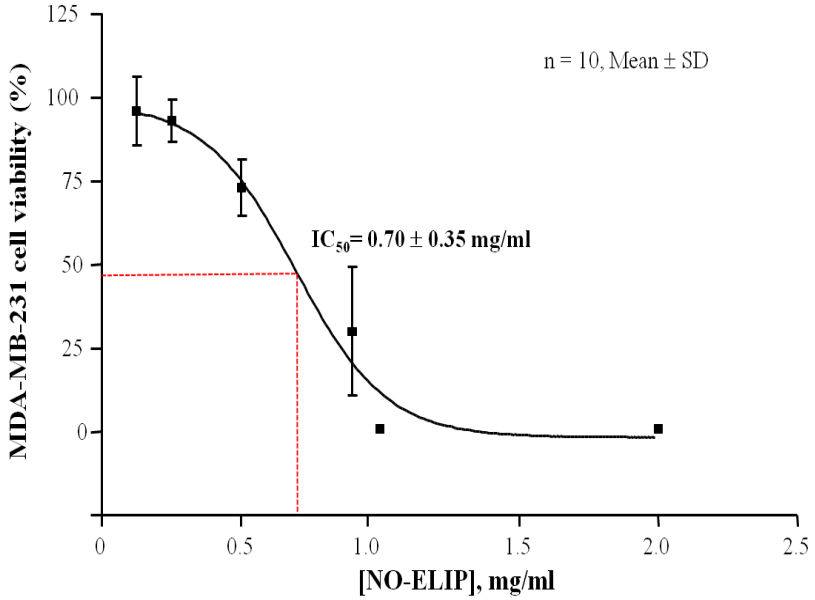

Figure 3.5 MDA-MB-231 cell viability with NO-ELIP in PBS

MDA-MB-231 cell viability was determined by MTT assay. Data are shown as mean ± standard deviation of MDA-MB-231 cell viability from ten independent experiments. The dose-response curve was generated. IC_{50} value of NO-ELIP in PBS was 0.70 ± 0.35 mg/ml.

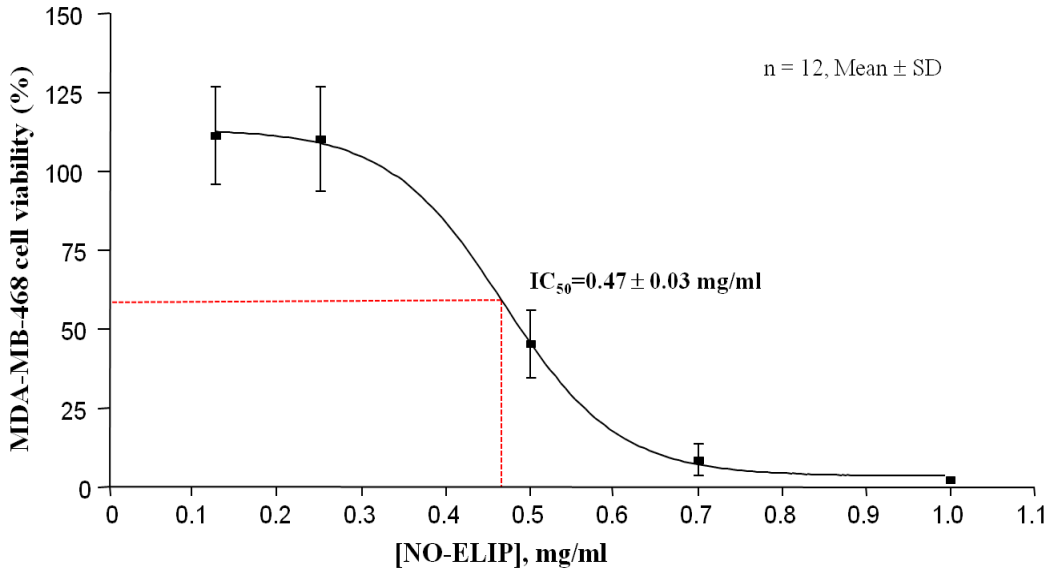

Figure 3.6 MDA-MB-468 cell viability with NO-ELIP in PBS

MDA-MB-468 cell viability was determined by MTT assay. Data are shown as mean ± standard deviation of MDA-MB-468 cell viability from twelve independent experiments. The dose-response curve was obtained. IC_{50} value of NO-ELIP in PBS was 0.47 ± 0.03 mg/ml.

3.2.4. Dose dependent BCC response to NO-ELIP resuspended in PBS/BSA

The effect of NO-ELIP resuspended in PBS/BSA on MDA-MB-231 cell viability is shown in Fig 3.7. At the concentration of 0.125 and 0.25 mg/ml of NO-ELIP resuspended in PBS/BSA, 60 % of MDA-MB-231 cells remained alive. The cytotoxic IC_{50} value of NO-ELIP was 0.5 mg/ml. MDA-MB-231 cell viability dramatically decreased with the concentration of 0.5 mg/ml. The data indicate that MDA-MB-231 cells respond to NO-ELIP concentration resuspended in PBS/BSA in a dose-dependent manner, and 0.5 mg/ml of NO-ELIP is the critical concentration to inhibit 50% MDA-MB-231 cell growth.

The dose response curve of MDA-MB-468 is shown in Fig 3.8. NO-ELIP in concentrations of 0.125 and 0.25 mg/ml reduced 80% of MDA-MB468 cell viability. NO-ELIP concentration of 0.41 mg/ml was determined as the cytotoxic IC_{50}. However, 20% of MDA-MB-468 cells were viable with 1 mg/ml of NO-ELIP treatment. The data indicate that MDA-MB-468 cells respond to NO-ELIP in a dose-dependent manner.

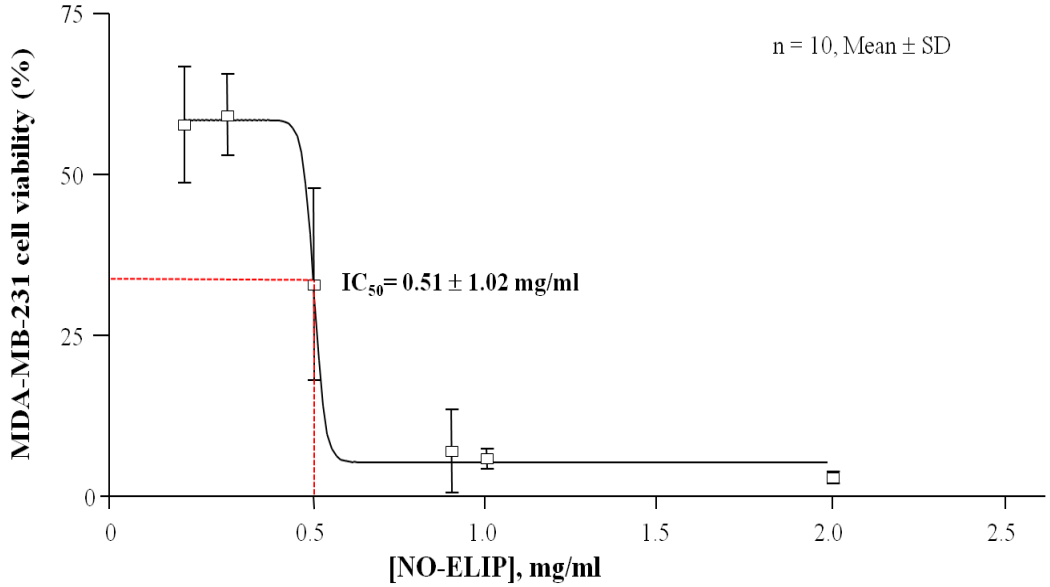

Figure 3.7 MDA-MB-231 cell viability with NO-ELIP resuspended in PBS/BSA

MTT assay was performed to determine MDA-MB-231 cell viability. Data are shown as mean ± standard deviation of MDA-MB-231 cell viability from ten different experiments. The dose-response curve was generated. IC_{50} value of NO-ELIP in PBS was 0.51 ± 1.02 mg/ml.

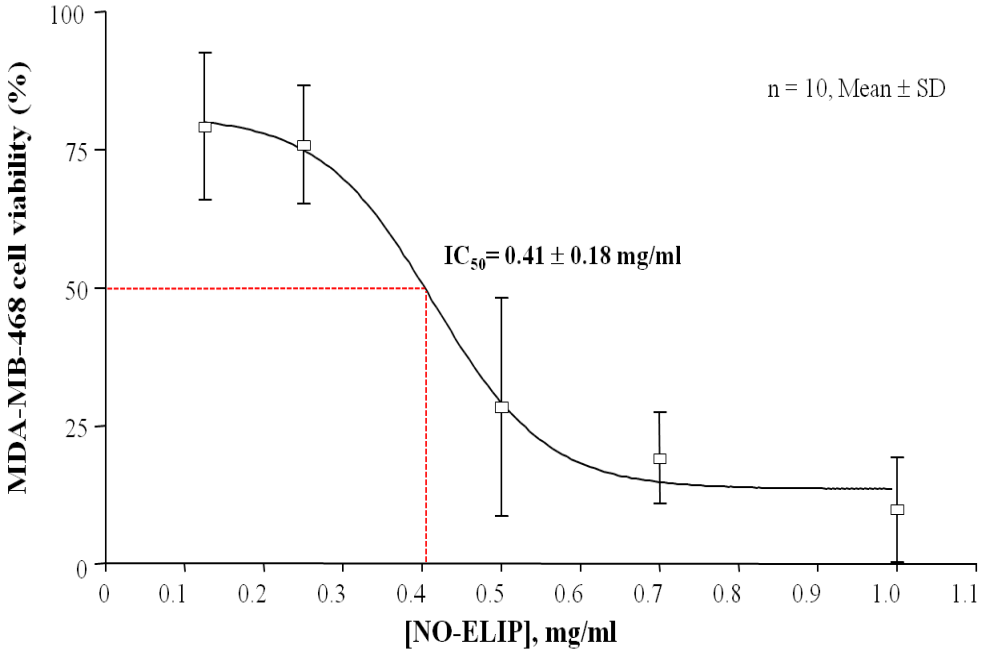

Figure 3.8 MDA-MB-468 cell viability with NO-ELIP resuspended in PBS/BSA

MTT assay was performed to identify MDA-MB-468 cell viability. Data are shown as mean ± standard deviation of MDA-MB-468 cell viability from four independent experiments. The dose-response curve was obtained. IC_{50} value of NO-ELIP in PBS was 0.41 ± 0.18 mg/ml.

3.3. Discussion

The data demonstrates that high levels of NO entrapped in NO-ELIP can induce cytotoxic effects on MDA-MB-231 and MDA-MB-468 after 5 hours of treatment. The specific aim of the study was to determine the efficiency of NO delivery strategy using NO-ELIP. The efficiency of NO delivery of two NO-donors such as spermine-NONOate and DETA-NONOate were compared with that of NO-ELIP. A MTT viability assay was conducted after the treatments with NO-donors and NO-ELIP to identify BCC viability.

The half life of Spermine-NONOate is 39 minutes at 37 ℃ (52). Approximately 50% of MDA-MB-231 cells underwent apoptosis with 656 μM of Spermine-NONOate in response to spontaneous NO release from Spermine-NONOate. The cytotoxic effects of approximately 50% of MDA-MB-468 cell death was produced by DETA-NONOate at 397 μM of concentration due to steady-state NO release with 20 hours of half-life at 37 ℃ (45). The concentration of NO-donors over the cytotoxic IC_{50} potentiated to effectively induce BCC death. There was a dose-dependent relationship between the concentration of NO generated by NO-donors and BCC viability.

NO-ELIP, the NO delivery carrier used in this study, induced a cytotoxic effect on BCCs in a dose-dependent manner. The improvement of NO-ELIP stability generated by the coating effect of BSA was determined by the comparison with NO-ELIP in the absence of BSA on BCC response. There was 28.6 % decrease in the cytotoxic IC_{50} value of NO-ELIP in the presence of BSA on MDA-MB-231 cell viability. MDA-MB-468 cells responded to NO-ELIP resuspended in BSA with 12.8 % decrease in its cytotoxic IC_{50} concentration. These results indicate that BCCs are more sensitive to NO-ELIP resuspended with PBS/BSA. It can be assumed that MDA-MB-231 are more sensitive than MDA-MB-468 in regard to cell death. However, higher concentrations of the cytotoxic IC_{50} are required for MDA-MB-231 due to its highly metastatic characteristic.

The use of NO-ELIP was effective to regulate the amount of NO delivered to BCCs and in prohibiting NO from being scavenged by hemoglobin in the systemic circulation (41). Decrease of NO exposure time during systemic delivery is crucial to reduce reaction with oxygen followed by the formation of nitrite (NO_2). NO_2 induces cytotoxicity in non-malignant cells and in the microenvironment (41). This study demonstrated that NO can be packaged using NO-ELIP and delivered to BCCs for NO-induced cytotoxic effect. The cytotoxic IC_{50} value of NO-ELIP may provide a therapeutic index of NO-ELIP for breast cancer treatment.

CHAPTER 4

Specific Aim 3 - Enhancement of NO Release with Ultrasound Application

4.1. Materials and Methodologies

4.1.1. Ultrasound-triggered NO release from NO-ELIP

An ultrasound-triggered NO release study was performed with the experimental setup as shown in Fig 4.1 (40). The setup was made up of a transwell insert allowing to hold NO-ELIP solution inside the transwell (30). Eight hundred microliter of NO-ELIP was introduced inside the transwell. The bottom of the transwell insert was made up of 0.4 μm pore polyester membrane. The transwell insert was placed on an acoustic absorber to eliminate acoustic reflectivity (23). A layer of water was placed between the transwell insert and the acoustic absorber to remove the air interference and avoid ultrasound reflection. Sonitron 1000 (Rich Mar Inc, TN, USA) was utilized with ultrasound parameters of 1 MHz, 1 W/cm^2 intensity and 100% duty cycle for 10 seconds of duration using a probe size with 1.2 cm diameter. Ten minutes after thawing the NO-ELIP, they were exposed to mechanical ultrasound. Right after the ultrasound was applied, echogenicity was measured using IVUS imaging for 5 hours.

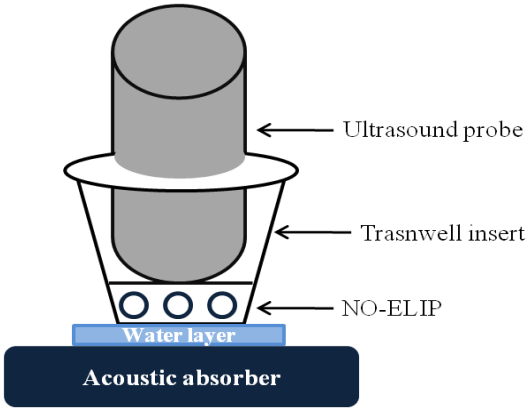

Figure 4.1 Experimental setup for ultrasound-triggered release study (40)

Adapted from Huang, S. L.

Resuspended NO-ELIP were introduced into the transwell insert. The use of the acoustic absorber and water layer allowed to remove the air interference and avoid ultrasound reflectivity. Ultrasound was applied and echogenicity of N-ELIP was measured.

4.1.2. Measurement of echogenicity of NO-ELIP

NO-ELIP were reconstituted to a lipid concentration of 0.1 mg/ml. The release of NO from NO-ELIP was measured using IVUS imaging at 0, 10, 20, 30, 60, 120, 180, 240, and 300 minutes. Fifty microliters of NO-ELIP collected from the transwell after ultrasound application put in 5 ml of PBS/BSA in a 12×16 glass vial at room temperature (21 to 22 ℃). The IVUS imaging catheter was inserted into the glass vial containing reconstituted NO-ELIP. IVUS imaging was performed at different time points with fixed instrumental setting such as gain, zoom, and reject. At each time point, an IVUS image of reconstituted NO-ELIP was recorded in real time. The regions of interest in the recorded images were manually traced between the vial wall and the imaging catheter to calculate MGSV (23). MGSV was computed using the Image-Histogram function in Image-Pro Plus software (Version 4.1, Media Cynernetics, Silver Spring, MD). Background MGSV of PBS/BSA was determined as the lower limit of the measurement. The MGSV measurement of NO-ELIP were reduced by the background value of MGSV (23). In order to identify ultrasound-triggered NO release from NO-ELIP, the percentage retention of MGSV was calculated using the initial MGSV of each sample regarded as 100%. The MGSV of each time point was divided by the initial MGSV and multiplied by 100. Therefore, MGSVs of NO-ELIP were normalized to percentage retention. The percentage retention of MGSV of six samples were averaged.

4.2. Results

4.2.1. Ultrasound-triggered NO release from NO-ELIP

Ultrasound application improved NO release from NO-ELIP compared to spontaneous NO release. Comparison of the percentage retention of echogenicity of NO-ELIP with (■) and without (□) ultrasound application is depicted in Fig. 4.2. The top line indicates the percentage retention of echogenicity of NO-ELIP without ultrasound application. The bottom line represents the percentage retention of echogenicity of NO-ELIP with ultrasound application. Ultrasound application performed 10 minutes after the reconstitution of NO-ELIP caused significant increase in NO release from NO-ELIP. Ultrasound application enhanced NO release at 10 minute as depicted in Fig 4.3. The black bar indicates the MGSV of NO-ELIP without ultrasound application. The gray bar represents the MGSV of NO-ELIP with ultrasound application. NO-ELIP without ultrasound application showed higher echogenicity with a MGSV of 116 ± 18. However, MGSV of NO-ELIP with ultrasound application was reduced to 71 ± 16. There was an average of 26% increase in NO release from NO-ELIP with ultrasound application.

Although NO-ELIP were exposed to ultrasound only one time, the loss of echogenicity with ultrasound application was significantly increased ($p < 0.05$). The echogenicity of NO-ELIP with ultrasound application dramatically decreased and almost disappeared at 2 hours. However, the decrease in NO-ELIP echogenicity without ultrasound application was steady up to 5 hours. The results demonstrate that there was ultrasound-triggered release of NO from NO-ELIP, indicating ultrasound application can improve NO release from NO-ELIP.

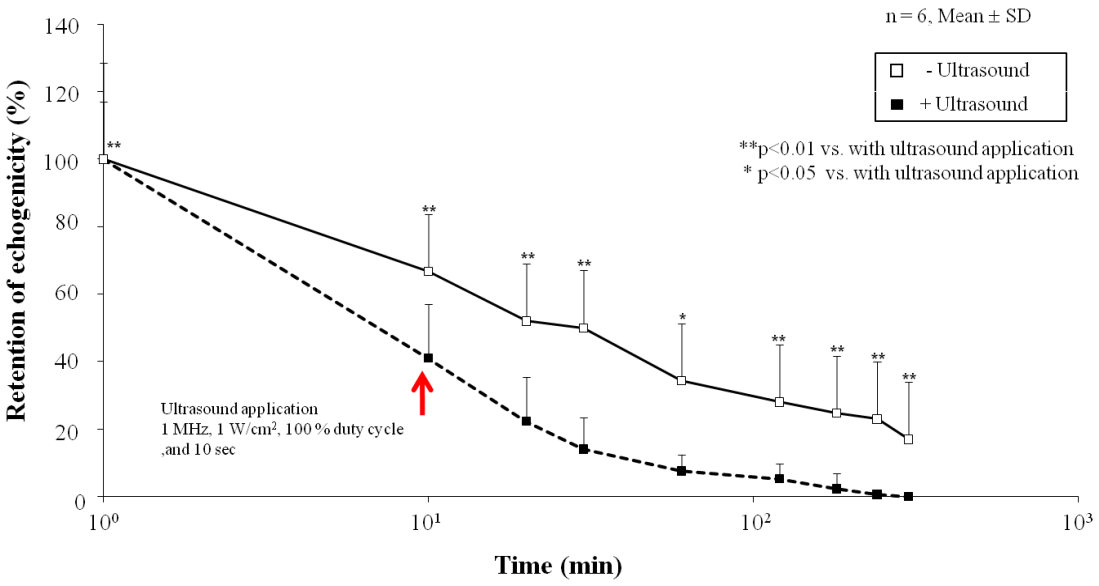

Figure 4.2 Percent retention of echogenicity of NO-ELIP with and without ultrasound application

This graph illustrates percentage of retention of echogenicity at different time points. Red arrow indicates the time point of ultrasound application 10 minutes after NO-ELIP reconstitution. This ultrasound-triggered NO release study was carried out with the use of ultrasound parameters of 1 MHz, 1 W/cm^2 and 100% duty cycle for 10 seconds of duration. After ultrasound application, echogenicity of NO-ELIP was measured by IVUS imaging. The top line indicates percentage retention of NO-ELIP without ultrasound application. The bottom line represents the percentage retention of NO-ELIP with ultrasound application. Results are represented as mean ± standard deviation from six independent experiments. These results showed significant difference ($p < 0.05$).

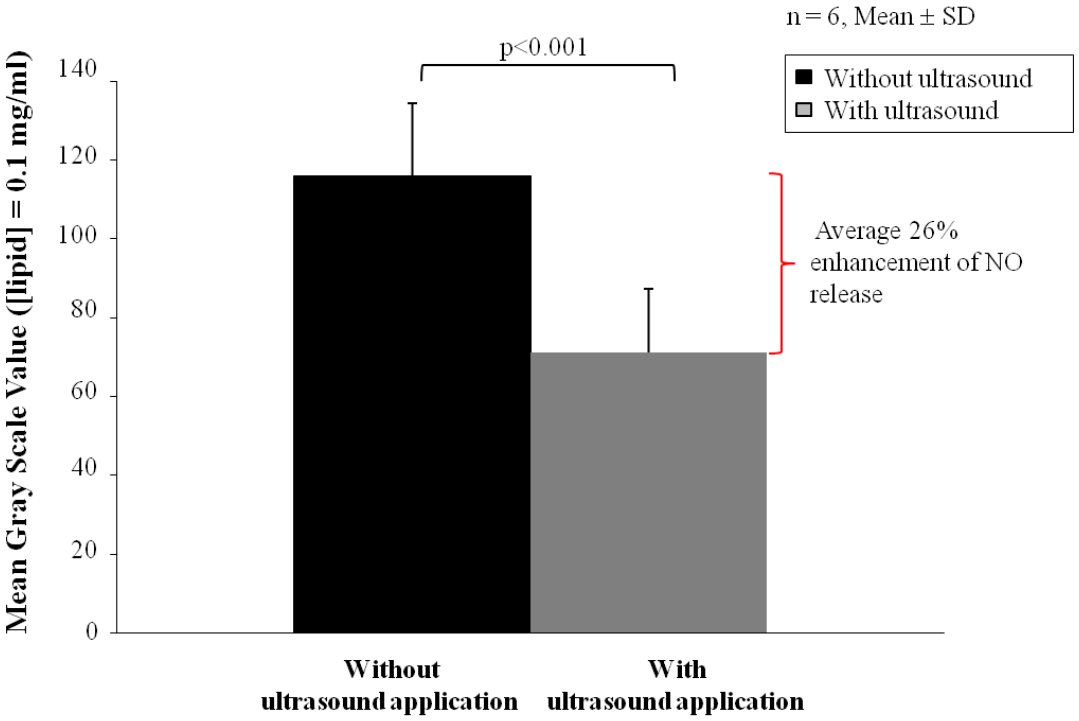

Figure 4.3 MGSV of NO-ELIP with and without ultrasound application

This bar graph clearly represents the comparison of MGSV at the 10 minutes time point with and without ultrasound application. Black bar indicates the MGSV of NO-ELIP without ultrasound application. Gray bar represents the MGSV of NO-ELIP applied ultrasound at 10 minutes. Results are shown as mean ± standard deviation from six independent experiments. These results showed a significant difference ($p < 0.001$).

4.3. Discussion

The principal objective of this chapter was to investigate ultrasound-triggered NO release from NO-ELIP and to evaluate the enhancement of NO release efficiency with ultrasound stimulation. The hypothesis is that ultrasound can enhance NO release from NO-ELIP.

Ultrasound was applied to thawed NO-ELIP 10 minutes after thawing process with ultrasound parameters of 1 MHz, 1 W/cm^2, and 100 % duty cycle for 10 seconds of duration time. NO release from NO-ELIP was quantitated by measuring echogenicity in IVUS images. Decrease of echogenicity of NO-ELIP after ultrasound application indicates increase of NO amount liberated from NO-ELIP stimulated by ultrasound application. The rapid decrease in NO-ELIP echogenicity was observed at 10 minutes. Echogenicity of NO-ELIP disappeared 2 hours after ultrasound application. The results indicate that ultrasound application induces an average of 26 % enhancement of NO release from NO-ELIP.

Ultrasound-triggered gas diffusion is determined by liposomal composition, the encapsulated gas properties, and ultrasound parameters (30). It was hypothesized that ultrasound can induce oscillation behavior of liposomes and force NO diffused from NO-ELIP at a low acoustic power. Ultrasound-controlled NO release has the potential to be utilized for targeted monotherapy of breast tumor treatment (54).

Ongoing research has demonstrated ultrasound-induced release of air and other inert gases from ELIP (33). To investigate the mechanism of NO release from NO-ELIP using ultrasound application, direct measurement of the NO amount diffused out of NO-ELIP must be evaluated in future research. The most crucial ultrasound characteristics are correlated with power input and duration of Sonication effects (37). Ultrasound parameters need to be optimized to maximize the NO release profile from NO-ELIP.

CHAPTER 5

Summary and Future Directions

5.1. Summary

NO-ELIP have the potential not only to encapsulate and deliver NO to BCCs, but also to control NO release via direct ultrasound exposure. The present study includes a number of in-vitro studies to demonstrate the efficiency of NO-ELIP as NO gas delivery agent for BCC treatment. First, the stability of NO-ELIP over time was investigated with the measurement of echogenicity using ultrasound imaging. Secondly, NO dose-dependent response of BCCs with two known NO donors were determined and compared to those with NO-ELIP. Lastly, ultrasound-controlled NO release from NO-ELIP was evaluated by ultrasound application utilizing the measurement of echogenicity.

As described in Chapter 2, the echogenicity of NO-ELIP resuspended in PBS/BSA was more stable than that of NO-ELIP in PBS up to 5 hours. This result may provide important information as to design experiments of NO-ELIP treatment for BCCs. BCCs were exposed to NO-ELIP for 5 hours in order for NO-ELIP to generate a cytotoxic effect on BCCs viability.

The utility of NO-donors verified the NO dose-dependent characteristics of the BCCs. The effect of NO-ELIP on BCC death was highly dependent on concentration compared with that of NO-donors in Chapter 3. In order to demonstrate NO-induced cell death, NO-saturated mannitol solution and empty ELIP were used to investigate NO-induced cytotoxicity on BCCs. This study revealed that NO-induced cytotoxicity was not by lipid effect, but mainly by NO.

Chapter 4 shows that NO-ELIP were able to liberate encapsulated NO triggered by ultrasound application. There was an average of 26 % enhancement of NO release from NO-ELIP after applying ultrasound. Ultrasound application induces a rapid NO release rate from NO-ELIP.

In this study, a unique cytotoxic gas delivery system using NO-ELIP has been developed for breast cancer treatment. NO-ELIP can encapsulate NO gas more stably with the improvement of purified NO gas injection. The use of BSA enhances NO-ELIP stability and

induces a stable rate of NO release. Cytotoxic efficacy of NO released from NO-ELIP on BCC viability was determined and compared with NO-donor treatments for the BCCs. Ultrasound application over NO-ELIP can enhance the rate of NO release.

5.2. Future directions

Previous research demonstrated that stead-state release of NO is more effective for generating programmed tumor cell death (49). The spontaneous NO release from NO-ELIP, in an initially rapid and then later slower pattern, may limit the cytotoxic effect of NO-ELIP on BCC viability. The enhancement of prolonged NO release from NO-ELIP is needed for further investigation with modification of lipid shell composition. The use of 50 mole % of DPPG may enhance the echogenicity and the toxic effect of NO-ELIP. Positively charged NO-ELIP with further optimized DC-Cholesterol·HCl mole % may improve the interaction between NO-ELIP and BCCs and enhance the efficacy of NO delivery to BCCs.

It has been shown that the presence of mannitol in the freezing step is essential for the preparation of gas-containing liposomes (40). The freezing mannitol solution generates lipid fusion followed by the formation of a gas bubble in the lipid bilayer. The use of mannitol not only improves encapsulation efficiency of gas but also enhances echogenicity (23). However, the use of mannitol was less effective for increasing permeability through the BCC membrane. Other carbohydrates and surfactants may be utilized to enhance the permeability of NO-ELIP to BCC. Moreover, NO-ELIP conjugated to specific biomarkers of BCCs such as Her-2, ER, PR, and EGFR may increase the permeability of NO-ELIP through the BCC membrane and provide targeted NO gas delivery.

In the present study, NO release from NO-ELIP was indirectly quantitated using IVUS images. We assumed that loss of echogenicity from NO-ELIP would correspond to NO release

from NO-ELIP due to ultrasound responsive characteristic of NO and NO-ELIP. The amount of NO encapsulated into NO-ELIP needs to be directly measured by a chemiluminescence technique to identify the therapeutic index of detrimental NO concentration for breast cancer treatment.

Ultrasound parameters need to be optimized for an improved NO release profile from NO-ELIP and improved efficacy of NO-ELIP as ultrasound contrast agent. Ultrasound-triggered spatial and temporal NO releases needs to be evaluated through in-vivo experiments for targeted monotherapy of breast tumor treatment. The application of clinical Doppler ultrasound may improve the therapeutic effect of NO-ELIP as a toxic agent delivery carrier. In order to improve ultrasound effect on the mechanism of NO release, the sensitivity of NO-ELIP to ultrasound may be enhanced with modification of lipid formulation. BCC response to ultrasound-driven NO release needs to be studied to verify the enhancement of NO-ELIP on therapeutic application.

References

1. Jemal, A., R. Siegel, J. Xu, and E. Ward. 2010. Cancer statistics, 2010. CA Cancer J Clin 60:277-300.
2. Baum, M., and H. Schipper. 2005. Breast Cancer. Fast fact.
3. Ferlay, J., C. Hery., P. Autier., and R. Sankaranarayanan. 2010. Global Burden of Breast Cancer. Springer Science Business Media.
4. Bertucci, F., and D. Birnbaum. 2008. Reasons for breast cancer heterogeneity. J Biol 7:6.
5. Hsiao, Y. H., M. C. Chou, C. Fowler, J. T. Mason, and Y. G. Man. 2010. Breast cancer heterogeneity: mechanisms, proofs, and implications. J Cancer 1:6-13.
6. Tu, S. 2010. Origin of Cancers: Clinical Perspectives and Implications of a Stem-Cell Theroy of Cancer. Springer.
7. Geddes, D. T. 2007. Inside the lactating breast: the latest anatomy research. J Midwifery Womens Health 52:556-563.
8. DiMeo, T. A., and C. Kuperwasser. 2006. The evolving paradigm of tissue-specific metastasis. Breast Cancer Res 8:301.
9. Tanaka, T., P. Decuzzi, M. Cristofanilli, J. H. Sakamoto, E. Tasciotti, F. M. Robertson, and M. Ferrari. 2009. Nanotechnology for breast cancer therapy. Biomed Microdevices 11:49-63.
10. Singh, M. S., P. A. Francis, and M. Michael. 2010. Tamoxifen, cytochrome P450 genes and breast cancer clinical outcomes. Breast 20:111-118.
11. Umesono, K., and R. M. Evans. 1989. Determinants of target gene specificity for steroid/thyroid hormone receptors. Cell 57:1139-1146.
12. Weigelt, B., J. L. Peterse, and L. J. van 't Veer. 2005. Breast cancer metastasis: markers and models. Nat Rev Cancer 5:591-602.
13. Aapro, M. S. 2001. Adjuvant therapy of primary breast cancer: a review of key findings from the 7th international conference, St. Gallen, February 2001. Oncologist 6:376-385.

14. Sverrisdottir, A., H. Johansson, U. Johansson, J. Bergh, S. Rotstein, L. Rutqvist, and T. Fornander. 2011. Interaction between goserelin and tamoxifen in a prospective randomised clinical trial of adjuvant endocrine therapy in premenopausal breast cancer. Breast Cancer Res Treat.

15. Yau, T., H. Sze., I. S. Soong., F. Hioe., U. Khoo., and A. W. Lee. 2008. HER2 overexpression of breast cancers in Hong Kong: prevalence and concordance between immunohistochemistry and in-situ hybridisation assays. Hong Kong Med J 14:130-135.

16. Fendly, B. M., M. Winget, R. M. Hudziak, M. T. Lipari, M. A. Napier, and A. Ullrich. 1990. Characterization of murine monoclonal antibodies reactive to either the human epidermal growth factor receptor or HER2/neu gene product. Cancer Res 50:1550-1558.

17. Burstein, H. J. 2003. Trastuzumab in combination with chemotherapy. Breast Cancer Res Treat 81:S69-72.

18. Sparano, J. A., A. N. Makhson, V. F. Semiglazov, S. A. Tjulandin, O. I. Balashova, I. N. Bondarenko, N. V. Bogdanova, G. M. Manikhas, G. P. Oliynychenko, V. A. Chatikhine, S. H. Zhuang, L. Xiu, Z. Yuan, and W. R. Rackoff. 2009. Pegylated liposomal doxorubicin plus docetaxel significantly improves time to progression without additive cardiotoxicity compared with docetaxel monotherapy in patients with advanced breast cancer previously treated with neoadjuvant-adjuvant anthracycline therapy: results from a randomized phase III study. J Clin Oncol 27:4522-4529.

19. Sparano, J. A., and E. P. Winer. 2001. Liposomal anthracyclines for breast cancer. Semin Oncol 28:32-40.

20. Park, J. W. 2002. Liposome-based drug delivery in breast cancer treatment. Breast Cancer Res 4:95-99.

21. Di Paolo, A. 2004. Liposomal anticancer therapy: pharmacokinetic and clinical aspects. J Chemother 16 Suppl 4:90-93.

22. O'Brien, M. E., N. Wigler, M. Inbar, R. Rosso, E. Grischke, A. Santoro, R. Catane, D. G. Kieback, P. Tomczak, S. P. Ackland, F. Orlandi, L. Mellars, L. Alland, and C. Tendler. 2004. Reduced cardiotoxicity and comparable efficacy in a phase III trial of pegylated liposomal doxorubicin HCl (CAELYX/Doxil) versus conventional doxorubicin for first-line treatment of metastatic breast cancer. Ann Oncol 15:440-449.

23. Huang, S. L. 2010. Ultrasound-responsive liposomes. Methods Mol Biol 605:113-128.

24. Lodish, H., A. Berk, C. A. Kaiser., M. Krieger., M. P. Scott., A. Bretsher., H. Ploegh., and P. Matsudaira. 2007. Molecular Cell Biology.

25. Kwon, G. S., and T. Okano. 1996. Polymeric micelles as new drug carriers. Adv Drug Deliv Rev 21:107-116.

26. Shahin, M., S. Ahmed, K. Kaur, and A. Lavasanifar. 2011. Decoration of polymeric micelles with cancer-specific peptide ligands for active targeting of paclitaxel. Biomaterials 32:5123-5133.

27. Talelli, M., C. J. Rijcken, S. Oliveira, R. van der Meel, P. M. van Bergen En Henegouwen, T. Lammers, C. F. van Nostrum, G. Storm, and W. E. Hennink. 2011. Nanobody - Shell functionalized thermosensitive core-crosslinked polymeric micelles for active drug targeting. J Control Release 151:183-192.

28. Xiong, X. B., A. Falamarzian, S. Garg, and A. Lavasanifar. 2011. Engineering of amphiphilic block copolymers for polymeric micellar drug and gene delivery. J Control Release. In press.

29. Allison, S. D. 2007. Liposomal drug delivery. J Infus Nurs 30:89-95; quiz 120.

30. Huang, S. L. 2008. Liposomes in ultrasonic drug and gene delivery. Adv Drug Deliv Rev 60:1167-1176.

31. Dass, C. R., Choong, P. 2006. Selective gene delivery for cancer therapy using cationic liposomes: In vivo proof of applicability. J Control Release 113:155-163.

32. Lasic, D. D. 1997. Recent developments in medical applications of liposomes: sterically stabilized liposomes in cancer therapy and gene delivery in vivo. J Control Release 48:203-222.

33. Huang, S. L., and R. C. MacDonald. 2004. Acoustically active liposomes for drug encapsulation and ultrasound-triggered release. Biochim Biophys Acta 1665:134-141.

34. Buchanan, K. D., S. L. Huang, H. Kim, D. D. McPherson, and R. C. MacDonald. 2010. Encapsulation of NF-kappaB decoy oligonucleotides within echogenic liposomes and ultrasound-triggered release. J Control Release 141:193-198.

35. Chen, J. L., H. Wang, J. Q. Gao, H. L. Chen, and W. Q. Liang. 2007. Liposomes modified with polycation used for gene delivery: preparation, characterization and transfection in vitro. Int J Pharm 343:255-261.

36. Zasadzinski, J. A., B. Wong, N. Forbes, G. Braun, and G. Wu. Novel Methods of Enhanced Retention in and Rapid, Targeted Release from Liposomes. Curr Opin Colloid Interface Sci 16:203-214.

37. Smith, D. A., T. M. Porter, J. Martinez, S. Huang, R. C. MacDonald, D. D. McPherson, and C. K. Holland. 2007. Destruction thresholds of echogenic liposomes with clinical diagnostic ultrasound. Ultrasound Med Biol 33:797-809.

38. Huang, S., A. J. Hamilton, S. D. Tiukinhoy, A. Nagaraj, B. J. Kane, M. Klegerman, D. D. McPherson, and R. C. MacDonald. 2002. Liposomes as ultrasound imaging contrast agents and as ultrasound-sensitive drug delivery agents. Cell Mol Biol Lett 7:233-235.

39. Shung, K. K., D. Y. Fei, Y. W. Yuan, and W. C. Reeves. 1984. Ultrasonic characterization of blood during coagulation. J Clin Ultrasound 12:147-153.

40. Huang, S. L., A. J. Hamilton, A. Nagaraj, S. D. Tiukinhoy, M. E. Klegerman, D. D. McPherson, and R. C. Macdonald. 2001. Improving ultrasound reflectivity and stability of echogenic liposomal dispersions for use as targeted ultrasound contrast agents. J Pharm Sci 90:1917-1926.

41. Huang, S. L., P. H. Kee, H. Kim, M. R. Moody, S. M. Chrzanowski, R. C. Macdonald, and D. D. McPherson. 2009. Nitric oxide-loaded echogenic liposomes for nitric oxide delivery and inhibition of intimal hyperplasia. J Am Coll Cardiol 54:652-659.

42. Buchanan, K. D., S. Huang, H. Kim, R. C. Macdonald, and D. D. McPherson. 2008. Echogenic liposome compositions for increased retention of ultrasound reflectivity at physiologic temperature. J Pharm Sci 97:2242-2249.

43. Sonveaux, P., B. F. Jordan., B. Gallez., and O. Feron. 2009. Nitric oxide delivery to cancer: Why and how? Eur J Cancer 45:1352-1369.

44. Mocellin, S., V. Bronte, and D. Nitti. 2007. Nitric oxide, a double edged sword in cancer biology: searching for therapeutic opportunities. Med Res Rev 27:317-352.

45. Coulter, J. A., H. O. McCarthy, J. Xiang, W. Roedl, E. Wagner, T. Robson, and D. G. Hirst. 2008. Nitric oxide--a novel therapeutic for cancer. Nitric Oxide 19:192-198.

46. Hirst, D., and T. Robson. 2007. Targeting nitric oxide for cancer therapy. J Pharm Pharmacol 59:3-13.

47. Bonavida, B., S. Khineche, S. Huerta-Yepez, and H. Garban. 2006. Therapeutic potential of nitric oxide in cancer. Drug Resist Updat 9:157-173.

48. Ridnour, L. A., D. D. Thomas, C. Switzer, W. Flores-Santana, J. S. Isenberg, S. Ambs, D. D. Roberts, and D. A. Wink. 2008. Molecular mechanisms for discrete nitric oxide levels in cancer. Nitric Oxide 19:73-76.

49. Pervin, S., R. Singh, and G. Chaudhuri. 2001. Nitric oxide-induced cytostasis and cell cycle arrest of a human breast cancer cell line (MDA-MB-231): potential role of cyclin D1. Proc Natl Acad Sci U S A 98:3583-3588.

50. Hanahan, D., and R. A. Weinberg. 2000. The hallmarks of cancer. Cell 100:57-70.

51. Snyder, C. M., E. H. Shroff, J. Liu, and N. S. Chandel. 2009. Nitric oxide induces cell death by regulating anti-apoptotic BCL-2 family members. PLoS One 4:e7059.

52. Pervin, S., R. Singh, and G. Chaudhuri. 2008. Nitric oxide, N omega-hydroxy-L-arginine and breast cancer. Nitric Oxide 19:103-106.

53. Thompson, J., K. Finlayson, E. Salvo-Chirnside, D. MacDonald, J. McCulloch, L. Kerr, and J. Sharkey. 2008. Characterisation of the Bax-nucleophosmin interaction: the importance of the Bax C-terminus. Apoptosis 13:394-403.

54. Rapoport, N. Y., K. H. Nam, Z. Gao, and A. Kennedy. 2009. Application of Ultrasound for Targeted Nanotherapy of Malignant Tumors. Acoust Phys 55:594-601.

Appendices

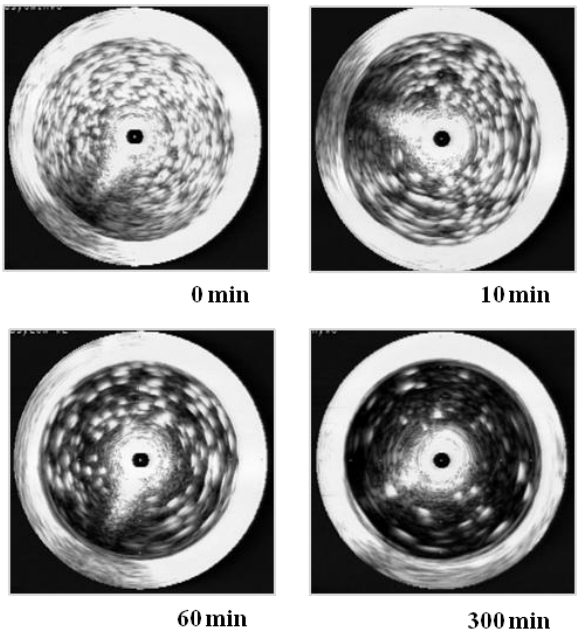

Figure A.1. IVUS images of NO-ELIP resuspended in PBS/BSA

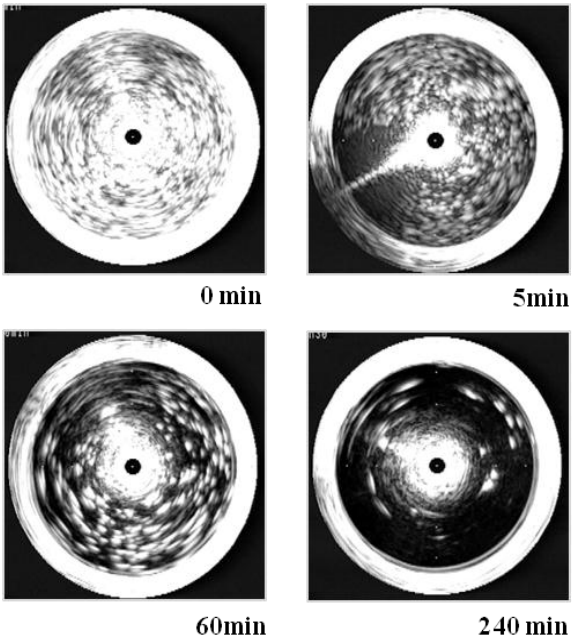

Figure A.2. IVUS images of NO-ELIP resuspended in PBS

Vitae

Soo Yeon Lee was born November 15, 1983 in South Korea. She attended the Department of Bio-Mechatronic Engineering at Sungkyunkwan University. During her undergraduate years, she studied for one year at the State University of New York at Buffalo as an exchange student. Enrolling at the SUNY for two semesters not only gave her more confidence in her English, but also enhanced her academic enthusiasm for biomedical sciences. A Bachelor of Science degree was conferred in August of 2008. As of late 2008, she joined General Motors-Daewoo Auto and Technology as a researcher. This working environment also entailed the application of biomedical engineering to improve human safety. She saw an opportunity to fulfill her interest in biomedical research by pursuing a master's degree in biomedical sciences at the UT-GSBS in August of 2009. She joined the laboratory of Dr. Hyunggun Kim, where she focused on ultrasound responsive liposomes as a drug and gas delivery carrier toward breast cancer research. The master's program has provided her with the opportunity to understand molecular biology, biochemistry, cancer cell biology, and cancer metastasis. As a result of these classes and laboratory experiences, she has a strong foundation of the sciences behind biomedical research.